



Hydrogen defects in feldspars: kinetics of D/H isotope exchange and diffusion of hydrogen species in alkali feldspars

Harald Behrens¹

Received: 11 May 2021 / Accepted: 25 June 2021 / Published online: 14 July 2021
© The Author(s) 2021

Abstract

Diffusion of hydrogen in natural alkali feldspars (Eifel sanidine and adularia from unknown locality) containing strongly bonded OH defects was investigated by D/H isotope exchange in the T range 600–1050 °C at ambient pressure and at elevated pressures up to 8 kbar. Runs at 1 atm were performed in a fused silica tube connected to a liquid D₂O reservoir at room temperature. In the high- pressure experiments samples were sealed with D₂O in gold capsules and processed up to 4 kbar in externally heated pressure vessels using Ar/D₂O as the pressure medium. Experiments at 6–8 kbar were performed in an internally heated gas pressure vessel using the double capsule technique to minimize isotopic contamination by the pressure medium. Diffusion coefficients were determined either by measuring concentration-distance profiles of OH and OD with an IR microscope or by measuring the total exchange of oriented plates after various run durations using a macroscopic IR technique. Both methods gave consistent data. D/H interdiffusion, $D_{D/H}$, is almost identical in the adularia and in the sanidine implying that the chemical composition and the degree of Al/Si disorder have minor influence on the hydrogen isotope exchange in alkali feldspars. Furthermore, no effect of crystallographic orientation was found for $D_{D/H}$ in both feldspars. $D_{D/H}$ in sanidine, however, depends on the thermal pre-treatment. Heating for several days at 900 °C leads to a lowering of D by a factor of 2.3, indicating a corresponding decrease in mobile hydrogen species. Data for sanidine pre-annealed at 900 °C are well described in the T range 600–1050 °C by

$$D_{D/H}(\text{m}^2/\text{s}) = 6.9 \cdot 10^{-6} \exp\left(\frac{-162 \text{ kJ/mol}}{R \cdot T}\right)$$

The diffusivity is strongly enhanced by water pressures ($P_{\text{H}_2\text{O}}$), i.e., in the range of 0–2 kbar. At $P_{\text{H}_2\text{O}} = 2$ kbar the following equation applies in the T -range of 645–800 °C:

$$D_{D/H}(\text{m}^2/\text{s}) = 1.2 \cdot 10^{-6} \exp\left(\frac{-131 \text{ kJ/mol}}{R \cdot T}\right)$$

Experiments with D₂O/CO₂ mixture of ratio 1:1 gave smaller exchange rates compared to pure D₂O fluids, confirming that that not the pressure but the water fugacity leads to the increase in the mobility of hydrogen species. At 720 °C and pressures of 4–8 kbar, chemical diffusivities of H₂O, $\tilde{D}_{\text{H}_2\text{O}}$, were determined by fitting the weighted sum of the absorbances of the OH and the OD band vs. distance. The $\tilde{D}_{\text{H}_2\text{O}}$ values are similar to those reported by Kronenberg et al. (Geochim Cosmochim Acta 60:4075–4094, 1996) for dehydration of Kristallina adularia at ambient pressure. It is concluded that in both cases high concentrations of H₂O molecules on interstitial sites govern the transport of hydrogen. Comparison of D/H interdiffusion to O diffusion in sanidine (Freer et al. in Phil Mag A75:485–503, 1997) implies that not only interstitial H₂O but also protons contribute to the transport of hydrogen under hydrothermal conditions. On the other hand, the high $D_{D/H}$ at ambient pressure is attributed to an interdiffusion of protons and Na⁺, which is supported by Na tracerdiffusion data for sanidine (Wilangowski et al. in Defect Diffus Forum 363:79–84, 2015). A basic conclusion of this research is that hydrogen storage capacity and

✉ Harald Behrens
h.behrens@mineralogie.uni-hannover.de

¹ Institut Für Mineralogie, Universität Hannover, Callinstr. 3,
30167 Hannover, Germany

hydrogen diffusion in feldspars are largely determined by extrinsic defects, such as substitutional defects (i.e., $\text{Al}^{3+} + \text{H}^+$ for Si^{4+}) and associates of water molecules with vacancies. The bonding of hydrogen species to the defects can vary greatly, depending on the genesis of the feldspars, so that quantitative predictions are difficult.

Keywords Alkali feldspar · Diffusion · Hydrogen isotopes · Defects · H_2O solubility

Introduction

Feldspars are the most abundant minerals in the Earth's crust and are widely distributed on other planetary bodies of the inner Solar System. Knowledge of their kinetic and mechanical behavior is a prerequisite for a better understanding of tectonic and rock-forming processes. Numerous studies have shown that the properties of feldspars are very strongly affected by H_2O which can be dissolved as trace element in the feldspar structure (Johnson 2006). Al, Si ordering and disordering kinetics in feldspars can be enhanced by orders of magnitude (Yund and Tullis 1980; Goldsmith 1991) as well as oxygen isotope exchange between feldspars and fluids (Yund and Anderson 1974; Giletti et al. 1978; Elphick et al. 1988; Farver and Yund 1990; Freer et al. 1997; Farver 2010) or NaSi-CaAl interdiffusion in plagioclase (Yund 1986; Baschek und Johannes 1995). Electrical conductivity in plagioclase is also enhanced by hydrogen species, probably by contributions of protons to the charge transport (Yang et al. 2012). Strong effects of water on deformation of feldspar minerals or aggregates and on frictional properties of feldspars were observed as well (Rybacki et al. 2006; Matsuda et al. 2019; Matsuda 2020), but may be partially related to melt formation (Matsuda 2020).

Insights into the dynamics of hydrogen species and their influence on intracrystalline processes in feldspars can be obtained from diffusion studies. Large differences of the dehydration rates by more than three orders of magnitude have been observed for an adularia from Kristallina, Switzerland (Kronenberg et al. 1996) and an andesine from Halloran Springs, USA (Johnson and Rossman 2013). These differences are probably due to a different genesis and, related to this, to a different way of incorporation of hydrogen into the feldspar structure. Adularia is a variety of potassium feldspar characterized by a pseudo-orthorhombic crystal form that occurs typically in low-temperature, hydrothermal environments (Smith 1974). The Kristallina adularia studied by Kronenberg et al. (1996) exhibits a complex IR spectrum with four bands at 3620, 3455, 3280 and 3090 cm^{-1} . After heating for several days at 800 °C, not only a strong decrease in the overall intensity of the bands but also a dramatic irreversible change in the band structure was observed by Kronenberg et al. (1996). They concluded that the initial spectrum of the adularia represents stationary hydrogen

defects that become unstable upon heating and transform into mobile species.

The andesine studied by Johnson and Rossman (2013) originated from a high-temperature basaltic tuff. The IR spectrum shows a broad OH stretching vibration band centered at 3400 cm^{-1} with the maximum intensity closely aligned with the crystallographic *a* axis. This kind of IR spectra is common to many igneous feldspars, including alkali feldspars and plagioclase other than low albite, and the associated defects are referred to as *type IIa OH* defects by Johnson and Rossman (2004) based on IR spectroscopic features. The term considers that hydrogen is preferentially present in the form of hydroxyl groups, as indicated by near-infrared spectroscopy. In contrast, H_2O molecules were the predominant hydrogen species in the adularia used by Kronenberg et al. (1996).

The characteristics of the IR bands of the andesine studied by Johnson and Rossman (2013) are preserved even after heating to 1000 °C for several days; only a uniform decrease in intensity with annealing time was observed. As recently shown for plagioclase, the removal of *type IIa OH* defects is at least partially reversible (Behrens 2021). Several tens of $\mu\text{g/g}$ H_2O could be stably incorporated into plagioclases at 1000 °C already at one bar water pressure. The recovery of the OH defects can be explained by an association with another defect already present inside the feldspar, possibly a vacancy on cation sites originating from incorporation of excess silica during crystallization of the feldspar in the magma chamber (Behrens et al. 1990; Behrens 2021).

In the present study, Eifel sanidines were used to gain new insights into the defect reactions and the mobility of hydrogen species in feldspars. A detailed description of these feldspars and their properties is given in the first paper of this series (Behrens 2021). In addition to the IR band at 3400 cm^{-1} , the Eifel sanidines show a band at 3050 cm^{-1} which is most intense in the direction perpendicular to (010) (Beran 1986; Johnson and Rossman 2004; Behrens 2021). Following Johnson and Rossman (2004), the associated defects are denoted as *type IIb OH* defects, i.e. OH groups are also predominant in the sanidines.

However, solubility experiments, in which the water content of feldspar sections was measured after annealing at controlled temperature and water pressure, provide strong evidence that two different defect types are present in Eifel sanidines (Behrens 2021). At ambient pressure and water pressures below 0.3 bar only the very strongly bonded

type IIb OH defect survived prolonged heating for several weeks at 1000 °C. A likely explanation for this defect is a substitution of Si^{4+} by $\text{Al}^{3+} + \text{H}^+$, a common hydrogen defect in quartz (Kats 1962). At water pressures above 0.5 bar an additional hydrogen-bearing defect is formed, most likely of similar kind as the *type IIa OH* defect common in igneous feldspars. The concentration of this defect strongly increases with increasing water pressure.

Using the sanidine, diffusion of hydrogen species can be studied on the same material at very different conditions. In D/H isotope exchange experiments at ambient pressure and low D_2O partial pressure, hydrogen self-diffusion occurs at roughly constant water content, i.e. in absence of a chemical potential gradient of H_2O . From a phenomenological point of view this corresponds to simple D/H interdiffusion, although the underlying diffusion mechanism is probably more complex. At elevated water pressures in the kbar range, D/H interdiffusion is superimposed by inward diffusion of the chemical component H_2O . While in the first case the dissociation equilibrium of the *type IIb OH* defects has major control on the transport of hydrogen isotopes, in the second case the dissociation equilibrium of the *type IIa OH* defects determines the isotope exchange rate. In order to test the general importance of the new experimental findings, a second Eifel sanidine and an adularia of unknown locality are studied for comparison. The adularia contains also *type IIa OH* defects and is distinctly different to the one of Kronenberg et al. (1996). Defect models are proposed to interpret the experimental data.

Experimental

Samples

Three natural potassium-rich alkali feldspar single crystals, two sanidines from the Eifel, Germany (labelled SV and S2) and one adularia from an unknown locality (labelled A1) were used in the D/H isotope exchange experiments. Large parts of the crystals are free of cracks or other visible imperfections (e.g. inclusions). A detailed description of the materials is given by Behrens (2021). The crystals were oriented and cut parallel to the main cleavage planes (001) and (010). Additionally, some sections perpendicular to the crystallographic *a*-axis were prepared to study the direction dependence of hydrogen diffusion. The orientation of the sections from sanidine was verified using the pleochroism of the OH absorption bands (Beran 1986). In the case of the adularia, the orientation of the crystallographic axis was identified by single crystal X ray measurements and by conoscopic observations (Behrens 2021).

Table 1 Composition of alkali feldspars used in the diffusion study

	Sanidine SV Volkesfeld, Eifel, Germany	Sanidine S2 Eifel, Germany	Adularia A1 Unknown locality
wt% oxides			
SiO_2	64.11	64.38	63.85
Al_2O_3	18.71	18.8	18.82
Fe_2O_3	0.17	0.18	0.21
CaO	<0.01	<0.01	<0.01
SrO	0.02	0.04	0.02
BaO	0.61	0.61	1.14
Na_2O	1.73	1.73	3.12
K_2O	14.48	14.53	12.36
Total	99.83	100.27	99.52
$\mu\text{g/g H}_2\text{O}$	129 ± 10	147 ± 8	128 ± 9
mol% feldspar components			
Ab	15.2	15.2	27.2
Or	83.7	83.8	70.8
An	0.0	0.0	0.0
Ce	1.1	1.1	2.0

wt% oxide is based on electron microprobe analyses. All iron is given as Fe_2O_3 . Water content was measured by IR spectroscopy using the calibration of Johnson and Rossman (2003)

Ab = $\text{NaAlSi}_3\text{O}_8$, Or = KAlSi_3O_8 , An = $\text{CaAl}_2\text{Si}_2\text{O}_8$, Ce = $\text{BaAl}_2\text{Si}_2\text{O}_8$

The chemical composition of the feldspars determined by multiple electron microprobe analysis (CAMECA CAMEBAX) is given in Table 1. Measurements performed with an IR microscope on several plates indicate that H_2O is homogeneously distributed in all the three feldspar crystals. The deviation of the local H_2O concentration from the average value was always below 5%. Furthermore, polarized spectra show that the pleochroism does not vary within the crystals. This is extremely important because different slabs of each crystal were used in the diffusion experiments.

A part of the samples was thermally pre-treated to eliminate or at least to reduce the mobile *type IIa OH* defects. For this purpose, samples were heated in air at 700–900 °C for up to 55 days.

Diffusion experiments

Two types of isotope exchange experiments were performed to study diffusion of hydrogen species in the feldspars:

- (1) A cuboid ($3 \times 3 \times 5 \text{ mm}^3$, the long side aligned parallel to the *a* axis) was held at the diffusion conditions for a fixed time. The surfaces had previously been finely ground with a 7 μm diamond disc. When possible, two slices were prepared from the crystal after the experiment to measure diffusion profiles in different crystallographic

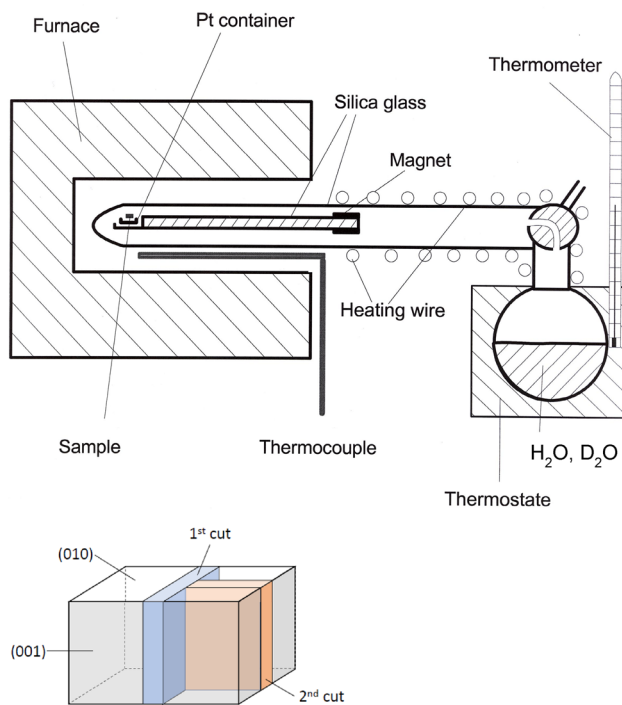


Fig. 1 Top. Scheme of the static setup used to control water pressure up to 1 bar. D₂O is used in D/H exchange experiments, H₂O in back-exchange experiments (H/D). Bottom. Illustration of preparation of cuboids for profiling. Depending on the crystal, the second cut was chosen to be either parallel to (001) or parallel to (010)

directions, as illustrated in Fig. 1 on bottom. First, a slice was cut in the centre parallel to the smallest plane (\perp a axis). Next, a second slab was cut parallel to one of the larger planes (\parallel (010) or \parallel (001)) out of the central region of a residual piece. In some cases, especially after high pressure experiments, only one section could be prepared due to mechanical damage of the cuboid. The plates were ground down to a typical height of 500 μm and polished on both sides. Using an IR microscope, profiles were measured on the sections from a surface of the cuboid towards the interior. The distance of the profile to the sides was kept as large as possible.

- (2) An alternative way to determine diffusion coefficients is to measure the isotopic composition of plates as a function of time. Double-side polished plates ($4 \times 4 \times 1$ mm) were heated in a D₂O-bearing atmosphere for a certain time, and changes in the IR spectra were analyzed after rapid cooling to room temperature. Bulk spectra were recorded in the central region of the plates, always with the same orientation of the plate to the IR beam. The heating process was repeated several times with increasing time intervals.

Most of the experiments were carried out at 1 atm. in a horizontal tube furnace using the setup shown in Fig. 1. The

sample holder consists of a silica rod (length: 200 mm) with a small platinum container at one end and a magnetizable steel piece at the other. After loading the sample in the Pt container, the sample holder was placed in the cold part of a silica tube. The tube end inside the furnace was closed, the other end was connected via a three-way stopcock to a glass bulb containing liquid D₂O (or H₂O in back exchange experiments). In the D/H exchange experiments, the glass bulb was at room temperature, and the water vapor pressure was about 25 mbar. Higher water pressures can be adjusted via a thermostat, as applied in the study on water solubility in feldspars (Behrens 2021).

To minimize H-isotopes in the gas, the silica tube was evacuated several times and refilled with air dried by bubbling through concentrated sulfuric acid. Thereafter, the tube was opened to the D₂O reservoir, and the sample was moved by magnetic coupling into the hot region of the furnace. The temperature was measured with a Pt/Pt90Rh10 (type S) thermocouple outside the tube a few mm away from the sample. The temperature at the sample position was tested by melting of NaCl or by inserting a shielded Ni/CrNi (K-type) thermocouple. Precision and accuracy of T was better than ± 5 °C in the 1 atm experiments. Heating of the samples to the target temperature took less than 1 min. After pulling out the specimen holder, the temperature dropped by more than 200 K within a few seconds.

High pressure runs were carried out in a cold seal pressure vessel (CSPV) at pressures up to 4 kbar and in an internally heated gas pressure vessel (IHPV) at higher pressures. In both cases argon was used as the pressure medium. Samples were loaded in gold capsules (5.4 mm outer diameter, 0.2 mm wall thickness, 25 mm length) and surrounded by powder from the same crystal to minimize non-isostatic stress during pressurization. Due to the high specific surface area, the powder also favors a rapid pre-saturation of the fluid with feldspar components. 5 wt% of D₂O were injected in the capsule before closing by arc-welding. Evaporation of D₂O was avoided by wrapping the capsule in tissue towels soaked in water and then frozen with liquid N₂. Capsules were checked for possible leakage by weighing after heating for at least 1 h at 105 °C.

The following procedure was chosen for the CSPV runs to minimize isotopic contamination during the experiment: After inserting the capsule into the autoclave 200 ml of D₂O were injected, and the autoclave was rapidly connected to the pressure line. Next, the autoclave was filled with 200–500 bar argon, depending on the target pressure, and disconnected from the pressure line during heating to the run temperature (duration: \approx 30 min.). When the temperature was reached, the desired pressure was established by short time opening the valve to the pressure line. During the experiment the autoclaves were separated from the pressure line.

The temperature during CSPV runs was measured with a K-type thermocouple in a bore hole at the end of the autoclave. The temperature distribution at the sample position was periodically calibrated using an autoclave equipped with three thermocouples in the interior. Uncertainty of T determination was ± 10 °C. Pressure was measured with a strain gauge manometer (accuracy ± 20 bar) at the beginning and at the end of each experiment. Loss of pressure during the experiments was always below 100 bar.

For the two experiments in an IHPV, the capsule containing the diffusion sample was inserted in a large gold capsule (8 mm inner diameter, 35 mm length). About 100 mg of D_2O were filled into the outer capsule as hydrogen isotopic buffer to minimize contamination of the inner capsule by hydrogen of the pressure medium which easily permeates through the capsule wall. Temperature was measured with four shielded K-type thermocouples adjacent to the capsule. Precision and accuracy of temperature was ± 10 K. Heating rate was 30 K/min over the last 200 K. Samples were isobarically quenched at an initial rate of 100 K/min after switching of the power of the furnace.

Infrared spectroscopy

IR absorption spectra were recorded using an FTIR spectrometer Bruker IFS88. The spectrometer provides a partial polarized beam which was always used to analyze samples from diffusion experiments. A globar source and a KBr beamsplitter were used in all measurements. 50–100 scans were accumulated for each spectrum with a spectral resolution of 2 cm^{-1} . Bulk measurements on crystal plates were performed within the spectrometer using an MCT (mercury cadmium telluride) detector. For this purpose, the samples were fixed on an aperture hole with a diameter of 1–2 mm, so that only the central region was analyzed.

In the early stage of the project, profiles were measured with an IR microscope Bruker A590, using a circular aperture corresponding to a focus diameter of 50 μm . For diffusion samples with thickness of 0.4–0.7 mm the effective diameter of the exited area was slightly larger (ca. 60 μm) as determined using an assemblage with a stepwise transition in OH concentration. Later, an IR microscope Bruker IRscope II was used, and an area 20–30 μm wide and about 100 μm long was set in the focus plane using a slit aperture. Aligning the long side parallel to the edge of the section, a spatial resolution of $\approx 40\text{ }\mu\text{m}$ could be achieved. Both microscopes are equipped with an MCT detector. Several profiles from older experiments were remeasured using the microscope IRscope II without significant difference in the obtained diffusion data.

On (010) or (001) sections, the prominent E vector of the partially polarized IR beam was always aligned parallel to the crystallographic a axis ($E_{dom} \parallel a$) to achieve a maximum intensity of the OH absorption band and, thus, to minimize

the error of species determination. For sections perpendicular to the a axis, the beam was oriented so that the E vector was perpendicular to (010) ($E_{dom} \parallel b$). Distance was measured with a digital xy stage with a precision of 0.1 μm . However, the uncertainty of distance measurements was much larger ($\pm 20\text{ }\mu\text{m}$) due to the applied slit aperture, but also due to slight tilting of the sections relative to the original surfaces, which could not always be completely avoided.

Results

Conditions and results of the diffusion experiments are summarized in Tables 2, 3. More details are given in the electronic supplements.

Spectra evaluation

An example of IR absorption spectra recorded along a profile after a D/H exchange experiment at ambient pressure is shown in Fig. 2a. In spectra with $E_{dom} \parallel a$, the maximum of the OH stretching vibration band is at 3400 cm^{-1} , and the OD stretching vibration band generated by hydrogen isotope exchange occurs at 2520 cm^{-1} . The OD band is superimposed by network vibration bands, i.e. on the low wavenumber side. To quantify the OD absorbance, a spectrum measured in the unchanged centre of the sample was subtracted from the spectra (Fig. 2b). The applied baselines for the determination of the respective peak heights are illustrated as dashed lines in Fig. 2a, b. The profiles of the absorbances for both bands (A_{OH} and A_{OD}) are consistent with an interdiffusion of D and H, i.e., the decrease of A_{OD} towards the interior is compensated by an increase of A_{OH} (Fig. 2c).

For the determination of the water contents C_w along the profiles by the Lambert–Beer law,

$$C_w = \frac{18.02 \cdot A_i}{d \cdot \rho \cdot \epsilon_i} \cdot 10^6, \quad (1)$$

the absorption coefficients ϵ_i must be known in addition to the density ρ and the thickness d . Here, C_w refers to the chemical component H_2O in $\mu\text{g/g}$, without consideration of the isotopy. The value of ϵ_{OH} could be derived from measurements on the natural sanidine SV (Behrens 2021). Adjusting $E_{dom} \parallel a$, the absorbance/thickness ratio A/d was $(0.217 \pm 0.007)\text{ mm}^{-1}$ for (010) sections [33 spectra] and $(0.173 \pm 0.006)\text{ mm}^{-1}$ for (001) sections [11 spectra]. With the density of $(2560 \pm 15)\text{ g/L}$ and the water content of $(129 \pm 10)\text{ }\mu\text{g/g}$ based on polarized IR spectroscopy (Behrens 2021), the ϵ_{OH} values are $(118 \pm 10)\text{ L mol}^{-1}\text{ cm}^{-1}$ for (010) sections and $(94 \pm 8)\text{ L mol}^{-1}\text{ cm}^{-1}$ for (010) sections. However, it must be emphasized that these ϵ_{OH} values are

Table 2 Conditions and results of H/D exchange experiments SV at ambient pressure (D in m^2/s)

No	Type	T (°C)	t (h)	Pre-treatment	Section	d (μm)	Direction a		Direction b		Direction c^*		Comment
							A_{Op}/A_{OH}	$\log D_D$	$\log D_H$	$\log D_D$	$\log D_H$	A_{Op}/A_{OH}	
Sanidine SV													
SV-E8	Profile	600	1320	7d 900 °C, air	(010)	447	0.810	-14.76	-14.75	0.820	-14.55	-14.79	
SV-D8	Profile	650	864	37d 900 °C, air	(010)	475	0.928	-14.21	-14.32		-14.41		
SV-E5	Profile	690	480	30d 700 °C, air	(010)	500	0.854	-13.54	-13.55	0.816	-13.46	-13.46	
SV-E6	Profile	690	480	30d 900 °C, air	(010)	500	0.887	-13.79	-13.80		-13.83		
SV-E15	Profile	720	168	14d 900 °C, air	perp a	500					-13.86		
SV-E14	Profile	720	168	14d 900 °C, air + 14d 720 °C, 2 kb H ₂ O	perp a	500				0.863	-13.35	-13.44	
SV-D7	Profile	720	290	27d 800 °C, air	(010)	475	0.863	-13.24	-13.35		-13.13		
SV-E11a	Profile	720	480	none	perp a	485					-13.20		
SV-E11b	Profile	720	480	7d 900 °C, air	(010)	393		-13.13			-13.18		
SV-E11c	Profile	720	480	55d 900 °C, air	(001)	400		-13.62			-13.52		
SV-E9	Profile	800	358	55d 900 °C, air	(010)	445		-13.67			-12.96	-12.89	Profile overlap in center
SV-DH4	t variat	800	-	23d 900 °C, air	(010)	958		-12.98			-12.88		
SV-D10	Profile	900	16	37d 900 °C, air	perp a	490		-12.88			-12.43		
SV-D10	Profile	900	16	37d 900 °C, air	(010)	490		-12.57			-12.31		High surface OH
SV-D5	Profile	900	67	7d 900 °C, air	(001)	402		-12.22					
SV-DH1	t variat	900	-	none	(010)	398	0.800	-12.24	-12.21				
SV-DH2a	t variat	900	-	23d 900 °C, air	perp a	1343	0.594	-11.95					
SV-DH2b	t variat	900	-	23d 900 °C, air	(001)	978	0.539	-12.18	-12.11				
SV-DH2c	t variat	900	-	23d 900 °C, air	(010)	958		-12.17	-12.14	0.616	-12.12	-12.10	
SV-HD3a	t variat	900	-	SV-DH2a	perp a	787	0.675	-12.46	-12.15				H/D back exchange
SV-HD3b	t variat	900	-	SV-DH2b	(001)	978				0.715	-12.31	-12.20	H/D back exchange
SV-HD3c	t variat	900	-	SV-DH2c	(010)	958				0.667	-12.41	-12.43	H/D back exchange
SV-DH9a	t variat	1000	-	SV-HD3a	perp a	787		-11.92					
SV-DH9b	t variat	1000	-	SV-HD3b	(001)	978					-11.92		
SV-DH9c	t variat	1000	-	SV-HD3c	(010)	958							
SV-E2	profile	1050	8	7d 900 °C, air	(001)	497		-11.28	-11.41	0.870	-11.49	-11.47	Profile overlap in center
SV-DH10a	t variat	1050	-	Multiple	(010)	957					-11.55		
SV-DH10b	t variat	1050	-	Multiple	(010)	957					-11.52		

Table 2 (continued)

No	Type	T (°C)	t (h)	Pre-treatment	Section	d (µm)	Direction a		Direction b		Direction c*		Comment
							A _{OD} /A _{OH}	log D _H	A _{OD} /A _{OH}	log D _H	A _{OD} /A _{OH}	log D _H	
SV-DH10c	t variat	1050	-	4d 900 °C, air	(010)	964			- 11.65				
SV-DH10d	t variat	1050	-	37d 900 °C, air	perp a	783	- 11.48						
Sanidine S2													
S2-C1	t variat	800	-	26d 900 °C, air	(010)	954			- 13.04				
Adularia A1													
A1-E1	t variat	800	-	35d, 900 °C, air	(010)	940			- 12.83				
A1-C1	t variat	900	-	35d, 900 °C, air	(001)	940			- 12.18				
A1-F1	t variat	900	-	A1-D1	(001)	942			- 12.53				
A1-G1	Profile	900	70	4d,900 °C, air	(010)	442	- 12.42		- 12.24				
					(010)	442	- 12.39		- 12.24				- 12.33
					perp a	442							- 12.33
					perp a	442							- 11.36
A1-D1	t variat	1050	-	A1-C1	(001)	940							

In the H/D back-exchange experiments a dynamic setup was used and air saturated with H₂O at ambient temperature was blown on the samples

specific for the IR spectrometer used in the present study, and other spectrometer may have a different degree of polarization of the IR beam.

The value of ε_{OD} can be obtained from the slope in a plot of A_{OH} against A_{OD} (Fig. 2d), if the total water content of the feldspars is constant. In Fig. 3a data of A_{OD}/A_{OH} are plotted for (010) and (001) sections in dependence on temperature. Samples pre-annealed at 900 °C are distinguished from those pre-annealed at lower temperature or without pre-treatment, since water loss is more likely for the second group of samples which still contain a high fraction of the mobile *type IIa OH* defects. However, no effect of pre-treatment or temperature on A_{OD}/A_{OH} is evident from Fig. 3a, and the average of 0.85 ± 0.05 derived from all data on the plot is suggested to represent ε_{OD}/ε_{OH}. Systematically higher values of A_{OD}/A_{OH} were obtained in experiments at elevated pressure (Fig. 3b), indicating an uptake of H₂O component from the fluid.

The ε_{OD}/ε_{OH} ratio of 0.85 was used to quantify the contribution of OD to the total water content by Eq. 1. In graphical illustrations of profiles, A_{OHtotal} (= A_{OH} + A_{OD}/0.85) is used as a proxy for the total water content (Figs. 2c, 4). An attempt to quantify C_w for sections perpendicular to the a axis was not done, because of the relatively high error of the low absorbances.

Determination of diffusivity using profiling

The absorbance-distance profiles were evaluated by the model of one-dimensional diffusion between an infinite reservoir (the gas phase) and a semi-infinite medium (the crystal) with the boundary condition of a constant surface concentration of the exchanged isotopes. Since the absorbance is proportional to concentration, the measured absorbance can be directly used for the determination of the diffusion coefficient. Assuming a constant diffusion coefficient D the solution of Fick's second law for these boundary conditions is

$$\frac{A - A_\infty}{A_s - A_\infty} = 1 - \text{erf} \frac{x}{\sqrt{4Dt}}, \tag{2}$$

where A is the absorbance at the distance x from the surface, A_∞ is the absorbance in the centre of the crystal, A_s is the absorbance at the surface and t is the run duration (Crank 1975). Profiles for A_{OH} and A_{OD} were independently fitted by Eq. (2). Typically, the data for ambient pressure are well reproduced by the fit curves, as shown in Fig. 2c. If the boundary conditions are fulfilled, the diffusion coefficients derived for both profiles (D_H and D_D) should be identical. For 12 profiles from experiments at 1 atm, both the A_{OH} and the A_{OD} profile were evaluated (see Table 2). Except for one very short profile (run SV-E8), D_H and D_D agree within 0.13 log units. Hence, the exchange process at 1 atm can be considered as simple D/H interdiffusion (D_{D/H}). Once this was

Table 3 Conditions and results of H/D diffusion experiments at elevated pressure (D in m^2/s)

No	p (kbar)	T ($^{\circ}\text{C}$)	t (h)	Pre-treatment	Sec-tion	d (μm)	Direction a			Direction b			Direction c*			Comment				
							$A_{\text{OH}}/A_{\text{OH}}$	$\mu\text{g/g}$ H_2O	$\log D_H$	$\log D_D$	$\log D_H$	$\log D_D$	$\log D_H$	$\log D_D$	$\log D_H$		$\log D_D$	$\log D_H$	$\log D_D$	$\log D_H$
Samidine SV																				
SV-E22	0.25	720	163	7d 900 $^{\circ}\text{C}$, air	(001)	488	1.050	116	-13.39	-13.43	1.145	122	-13.37	-13.40	0.987	89	-12.05	-12.10	-12.00	Profile overlap in centre
SV-E23	0.25	720	165	7d 900 $^{\circ}\text{C}$, air	(001)	477	1.128	110	-13.20	-13.24	1.000	100	-13.32	-13.26						
SV-E20	0.5	720	255	14d 900 $^{\circ}\text{C}$, air	perp a	458									0.987	89	-12.05	-12.10	-12.00	Profile overlap in centre
SV-D6	0.5	900	69	14d 900 $^{\circ}\text{C}$, 0.5 kbar H_2O	(010)	405	1.044	86	-11.95	-12.09	-12.53				1.030	89	-12.05	-12.10	-12.00	Profile overlap in centre
SV-E18	1	720	168	14d 900 $^{\circ}\text{C}$, air	(001)	443	1.058	138	-13.06	-13.12	-13.19									Profile overlap in centre
SV-E26	2	645	480	14d 900 $^{\circ}\text{C}$, air	(001)	485			-13.08		0.924	100	-13.36	-13.37	-12.85					
SV-E27	2	645	480	14d 900 $^{\circ}\text{C}$, air	(010)	504	0.982	130	-13.48	-13.55	-13.72				0.965	116	-13.83	-13.80	-13.51	$x_{\text{D}_2\text{O}}=0.51$
SV-E21	2	650	288	14d 900 $^{\circ}\text{C}$, air	(010)	485											-13.66			
SV-E16	2	725	168	14d 900 $^{\circ}\text{C}$, air	perp a	481									0.907		-12.63	-12.63		
SV-E17	2	725	168	14d 900 $^{\circ}\text{C}$, air	perp a	487					0.978		-12.91	-12.83	-12.14	1.004	-12.60	-12.58		
SV-E25	2	758	114	14d 900 $^{\circ}\text{C}$, air	(010)	512	1.187	125	-12.39	-12.45	-12.49				0.899		-12.60	-12.57		
SV-E24	2	758	114	14d 900 $^{\circ}\text{C}$, air	(010)	510	1.048	114	-12.53	-12.56					1.088	124	-12.64	-12.64	-12.51	
SV-180	2	800	8	none	(010)	703	1.155	137	-12.38	-12.31	-12.37				1.054	121	-12.72	-12.80	-13.03	$x_{\text{D}_2\text{O}}=0.51$
SV-E7	2	800	73	none	(010)	493	0.923	150	-12.41	-12.45	-12.65									

Table 3 (continued)

No	p (kbar)	T (°C)	t (h)	Pre-treatment	Sec-tion	d (µm)	Direction a			Direction b			Direction c*			Comment								
							A _{OH} /A _{Op}	µg/g H ₂ O	log D _H	log D _D	log D _{H2O}	A _{OH} /A _{Op}	µg/g H ₂ O	log D _H	log D _D		log D _{H2O}	A _{OH} /A _{Op}	µg/g H ₂ O	log D _H	log D _D	log D _{H2O}		
SV-E10	2	800	136	55d 900 °C, air	(010)	429	0.943	130	-12.45	-12.29		0.830	119	-12.26	-12.17	Profile overlap in centre								
SV-E19	4	720	76	14d 900 °C, air	perp a	453					1.261			-12.88	-13.00	-12.40	1.380			-12.69	-12.75	-12.95		
SV-E12	4	720	168	10d 900 °C, air	(010)	405	0.925	132	-12.94	-12.98	<i>-13.06</i>							1.150			-12.63	-12.72	-12.81	
SV-E28	6	720	40	none	(010)	696	1.310	159	-12.71	-12.61	-12.19							1.392	147	-12.42	-12.47	-12.11	IHPV, double capsule	
SV-E29	8	726	40	none	(010)	688	1.215	173	-12.32	-12.32	-12.11							1.090	149	-12.53	-12.61	-12.26	IHPV, double capsule	
Adularia A1																								
A1-E19	4	720	76	4d 900 °C, air	(010)	442	1.013		-12.92	-12.83	-12.36							1.172			-12.64	-12.63	-12.20	

Data for D_{H2O} printed in italics are only estimates and less reliable due to small uptake of H₂O

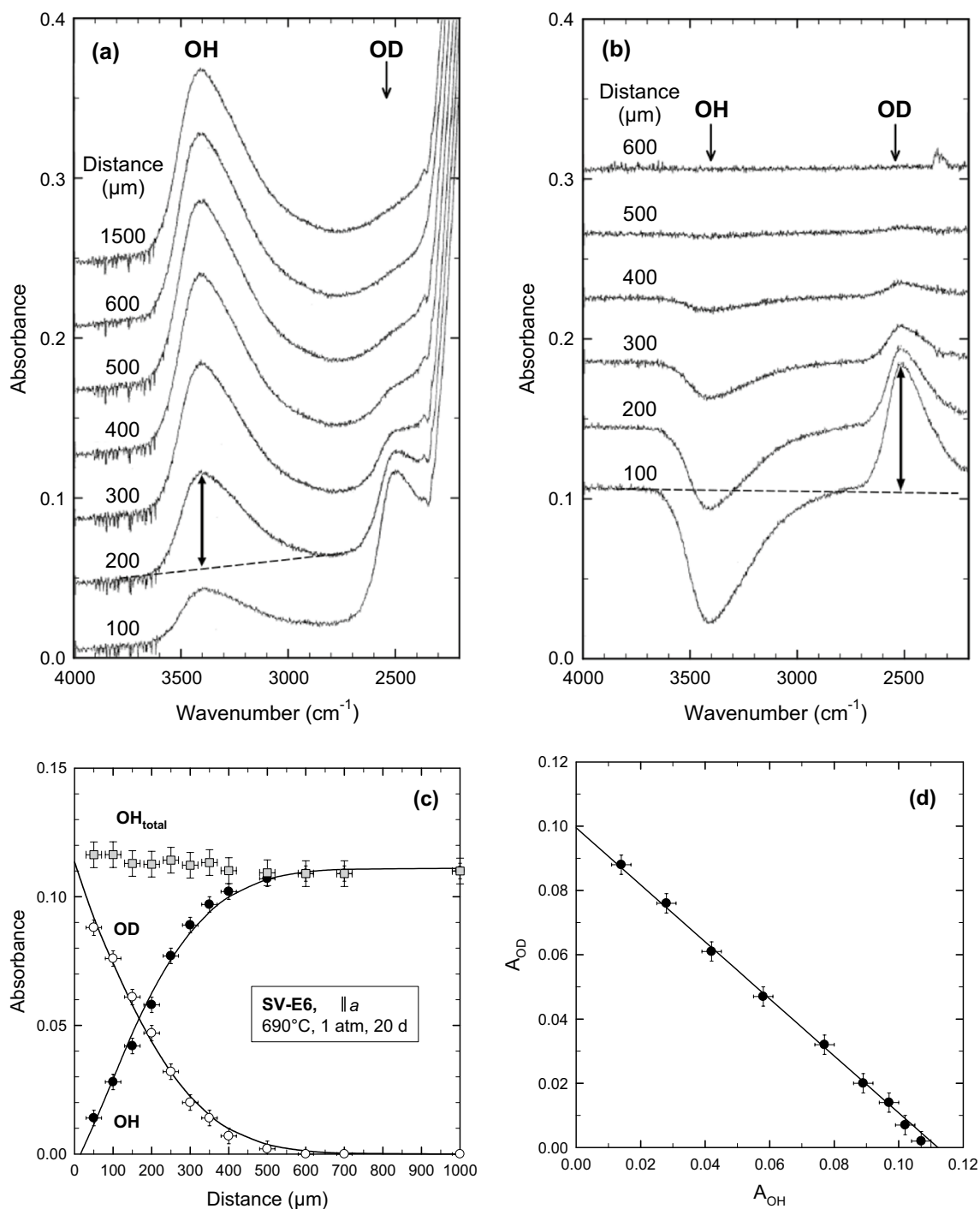


Fig. 2 Example of a D/H exchange experiment with a sanidine SV cuboid (Run SV-E6 for 20 days at 690 °C, $p_{\text{total}}=1$ atm, $p_{\text{D}_2\text{O}} \approx 25$ mbar). The profile was measured on a 500 μm thick (010) section along the crystallographic a axis, using a partially polarized beam with $E_{\text{dom}} \parallel a$. **a** IR absorption spectra recorded at selected distances from the surface. **b** Difference spectra obtained after subtraction of the spectra recorded at a distance of 1500 μm . **c** Profiles of the

absorbances of the OH peak and the OD peak. Baseline corrections used for the determination of the peak height (double arrow) are illustrated as dashed lines in the respective figures **(a)** and **(b)**. Solid lines are fits to the solution of Fick's 2nd law. The grey symbols represent the total water in the feldspar. $A_{\text{OH, total}} = A_{\text{OH}} + A_{\text{OD}}/0.85$. **d** Correlation between absorbance of OH and OD. The solid line represents a linear regression of the data. See text for details

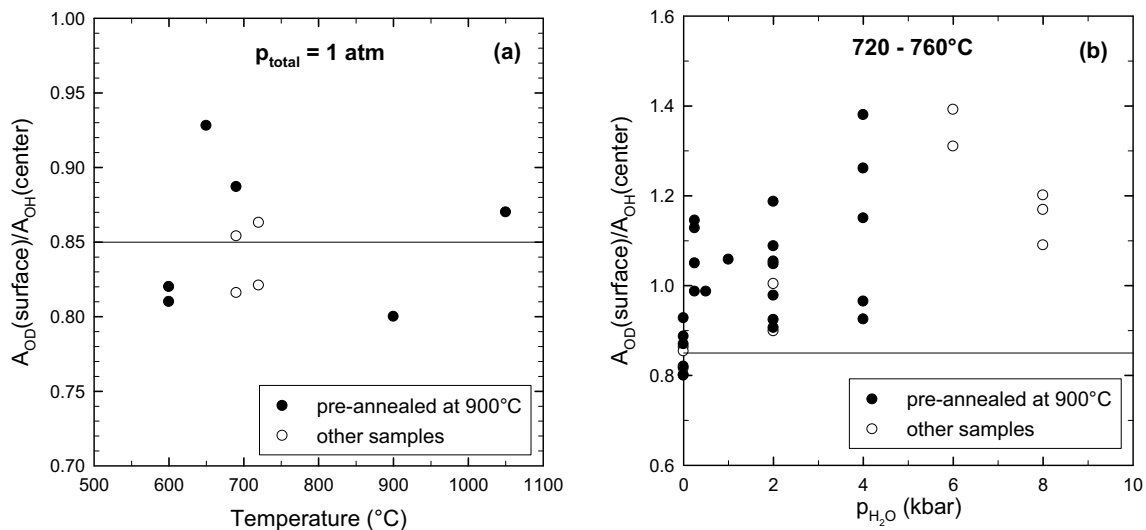


Fig. 3 Ratio of $A_{OD}(s)$, extrapolated to the surface, to $A_{OH}(c)$, measured in the center of the sample) for profiles recorded on sanidine SV after D/H exchange experiments. **a** At ambient total pressure and various temperatures. The average value of $A_{OD}(s)/A_{OH}(c)$ of 0.85 ± 0.05

established, only the OH profiles were usually evaluated due to time constraints. One needs to be aware that Eq. (2) is just a phenomenological description of the diffusion behavior. In this paper the term D/H interdiffusion refers to the 1:1 replacement of hydrogen by deuterium in the structure but does not mean that motion of hydrogen is directly coupled to the motion of deuterium. Alkalis can be involved as well in local charge compensation.

At elevated water pressures, noticeable deviation between measured absorbances and fit curves are observed both for A_{OH} and A_{OD} , marked by arrows in Fig. 4. These deviations are attributed to the uptake of hydrogen from the fluid, either as H_2O component or as protons, as indicated by the $A_{OHtotal}$ profiles. The effect is particularly pronounced at 4–8 kbar. An explanation is that the isotopic signature of the mobile hydrogen species is lost by exchange with the stationary OH defects at the beginning of the profile, and the mobile species at the front of profile contain basically only H but no D . Thus, the concept of D/H interdiffusion is only a rough approximation of the process, and the values of D_H and D_D obtained by fitting the concentration distance profiles with Eq. (2) have systematic errors. Despite this limitation, these data are useful for discussing the influence of water pressure on the diffusion of hydrogen species. For more in-depth modelling, the measured data are provided in the electronic supplement.

Only at pressures above 4 kbar the increase in total water content was large enough to evaluate the $A_{OHtotal}$ profiles with sufficient accuracy. In most cases, the $A_{OHtotal}$ profiles are also well fitted by Eq. (2), indicating that the chemical diffusion of hydrogen species in the sanidines is independent

is assumed to represent samples without change in total water content. **b** At high water pressure. Note that all high-pressure experiments are above the regression line, indicating uptake of water. See text for details

of C_w . This finding contrasts with numerous studies on H_2O diffusion in silicate glasses and melts which give clear evidence for a promoting effect of dissolved water on the H_2O diffusivity (see review of Zhang and Ni 2010). However, the increase in $A_{OHtotal}$ is relatively small even at 8 kbar and, considering the uncertainty in the determination of $A_{OHtotal}$, a weak dependence of hydrogen diffusivity on water content cannot be excluded.

Determination of diffusivity from bulk exchange experiments

In these experiments the bulk exchange of hydrogen isotopes between crystal plates and a surrounding gas phase was measured as a function of time. At constant surface concentration and constant diffusivity, the solution of Fick’s second law for a sheet of thickness d is given by Crank (1975)

$$\frac{M(t)}{M_\infty} = 1 - \frac{8}{\pi^2} \sum_{n=0}^{\infty} \frac{1}{(2n+1)^2} \cdot \exp\left(- (2n+1)^2 \cdot \frac{\pi^2}{d^2} \cdot Dt\right) \tag{3}$$

Here, $M(t)$ is the fraction of diffusing species that has left or entered the sheet after time t and M_∞ is the amount of the diffusing species that has left or entered the sheet after infinite time. In the initial stage of D/H exchange the fractional loss of hydrogen is proportional to the square root of time, and Eq. (3) can be converted to

$$\frac{A - A_\infty}{A_i - A_\infty} = \left(\frac{16 \cdot D}{\pi}\right)^{0.5} \cdot \frac{t^{0.5}}{d}, \tag{4}$$

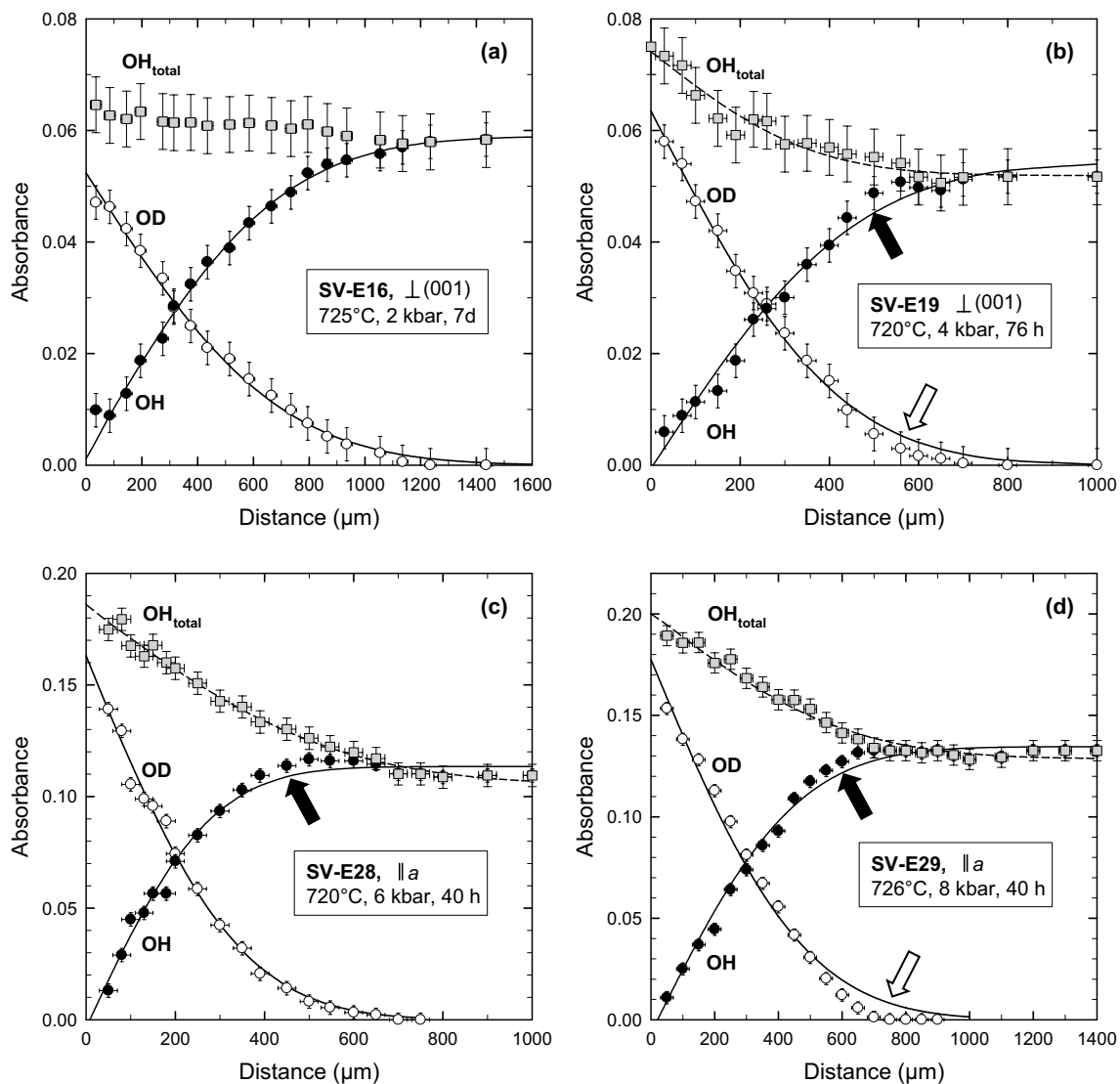


Fig. 4 a–d Examples of diffusion profiles recorded after D/H experiments with sanidine SV at elevated pressures and temperatures of 720–726 °C. The grey symbols represent the total water in the feldspar calculated using an $\epsilon_{OD}/\epsilon_{OH}$ ratio of 0.85. Lines are fits to the solution of Fick's 2nd law. Note deviations of A_{OH} and A_{OD} data from

the fit curve at greater depths for the highest water pressures (marked by arrows), which are attributed to the uptake of water by the samples. Agreement between the dashed fit curve for OH_{total} and the data indicate a constant diffusion coefficient of H_2O in these feldspars. See text for details

where A_i denotes the initial absorbance and A_∞ the final absorbance after infinite run duration.

The diffusion coefficients were determined by a linear regression from a plot of $(A - A_\infty)/(A_i - A_\infty)$ versus $t^{0.5}$ considering only the data with $(A - A_\infty)/(A_i - A_\infty) < 0.5$. In D/H exchange experiments, the evaluation of the A_{OH} data is straight forward with the assumption that $A_{OH,\infty}$ equals zero. Even if there is a slight change in the isotopic composition of the gas with time, this will not significantly affect the determined diffusion coefficients.

Evaluation of the OD band, however, requires the knowledge of absorbance of the band after complete exchange of D for H . Only in one experiment at 900 °C and 1 atm (SV-DH2,

see Table 2), both A_{OH} and A_{OD} were evaluated to determine the respective diffusion coefficients. This experiment serves as a test for the applicability of the method and the stability of OH defects under the prevailing conditions. Plates with three different orientations and thickness between 787 and 978 μm were used, which were previously annealed in air at 900 °C for 23 days to remove the mobile *type IIa* OH defects. Linear variation of absorbance with square root of time in the initial stage of the experiment is evident for both the OH band and the OD band (Fig. 5). After 354 h the OH band was no longer detectable in all sections, and the measured A_{OD} was assumed to represent $A_{OD,\infty}$. Using the

final absorbance values, D_H and D_D were determined by fitting the data to Eq. (4). The six diffusion coefficients agree within 0.11 log units (Table 2) confirming the equivalence of D_H and D_D for these conditions and the independence of diffusivity on crystallographic orientation.

Subsequently, the same samples were used in an H/D back-exchange experiment at the same temperature, with D_2O replaced by H_2O in the glass bulb (run SV-DH3). The OD band was no longer detectable after 200 h. A comparison of the OH absorbance with that before experiment SV-DH2 shows that the specimens have lost between 13 and 30% of their initial water content, with no correlation to thickness. The mean value of the diffusion coefficient is slightly lower for the D/H exchange experiment ($4.7 \times 10^{-13} \text{ m}^2/\text{s}$) than for the H/D exchange experiment ($7.3 \times 10^{-13} \text{ m}^2/\text{s}$), and the data scatter a bit more (within 0.31 log units). The results show that although the *type IIb* OH defects are not thermodynamically stable at 1 atm and a water partial pressure of 25 mbar, they have a sufficiently long lifetime to study the mobility of hydrogen species.

Methodical tests—effects of pre-treatment

Diffusion data obtained at 1 atm with sanidine SV are summarized in Fig. 6a. A systematic difference is visible between untreated or low-T annealed samples and samples pre-annealed at 900 °C in air. The influence of pre-annealing time was tested in an experiment at 720 °C (SV-E11). Two of the three cuboids were heated at 900 °C in air prior to the run, a smaller one ($2 \times 2 \times 4 \text{ mm}^3$) for 55 d, a larger one ($3 \times 3 \times 5 \text{ mm}^3$) for 7 d. A dehydration experiment yielded a diffusion coefficient of $1.4 \times 10^{-13} \text{ m}^2/\text{s}$ for sanidine SV at 900 °C (Behrens 2021). Based on this value, the characteristic diffusion length $(2Dt)^{0.5}$ is 0.41 mm after 7 days and 1.16 mm after 55 d. Accordingly, in the small cuboid, the mobile OH defects are mostly removed, while in the large cuboid this was achieved only in the outer region. The D_H values of both experiments agree within 0.15 log units (mean value of $2.4 \cdot 10^{-13} \text{ m}^2/\text{s}$) and are systematically lower than D_H determined for the untreated sample (mean value of $7.0 \times 10^{-13} \text{ m}^2/\text{s}$). Thus, the *type IIa* OH defects present in the natural sanidine have a strong attenuating effect on D/H interdiffusion. But heating for 7 days at 900 °C is sufficient to eliminate these defects in the diffusion zone.

Two experiments were performed to test whether the initial state of the sanidines can be recovered and how fast a new equilibrium concentration of mobile hydrogen defects can be achieved within a crystal. In each experiment two samples of SV were used. One sample was only pre-annealed for 14 days at 900 °C in air. The second one was heated afterwards for 14 days at 720 °C in an autoclave at 2 kbar water pressure. In the diffusion runs performed at 720 °C, either at ambient pressure or at 2 kbar D_2O pressure,

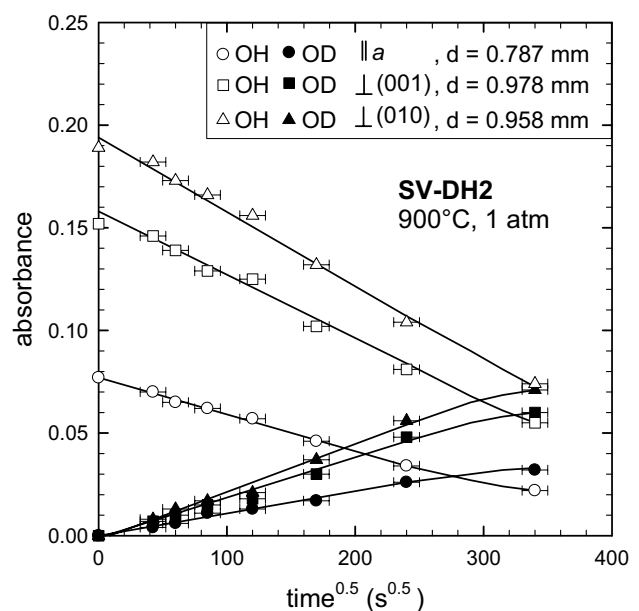


Fig. 5 Evolution of absorbances of OH and OD peaks with time during D/H exchange experiments with sanidine SV at 900 °C, $p_{\text{total}} = 1 \text{ atm}$, $p_{D_2O} \approx 25 \text{ mbar}$. The experiments were interrupted to measure spectra of the different sections at room temperature. The linear relationship between absorbance and square root of time was used to calculate the diffusion coefficients for the initial period of the exchange process

the D/H exchange rates were identical for both samples despite of the different pre-treatment (Tables 2, 3). Thus, the defect concentrations are established very fast in the diffusion zone of the crystal or, in other words, the diffusivity of the mobile hydrogen defects is considerably higher than the experimentally determined D/H interdiffusion coefficient. Ignoring the small difference in temperature, the diffusivity is higher by a factor of 1.9 at 2 kbar compared to ambient pressure which implies a correspondently higher concentration of mobile hydrogen defects in the zone of the hydrogen isotope exchange.

Temperature dependence of D/H interdiffusion in sanidine

The data in Fig. 6 also give strong evidence that D/H interdiffusion ($D_{D/H}$) is isotropic in the sanidine. All data for 900 °C pre-annealed samples, including the H/D back exchange runs, in the temperature range of 600–1050 °C are very well described with an Arrhenius equation

$$D_{D/H} = D_0 \cdot \exp\left(\frac{E_a}{R \cdot T}\right) \quad (5)$$

Values of the pre-exponential factor D_0 and the activation energy E_a are given in Table 4. The fit standard error

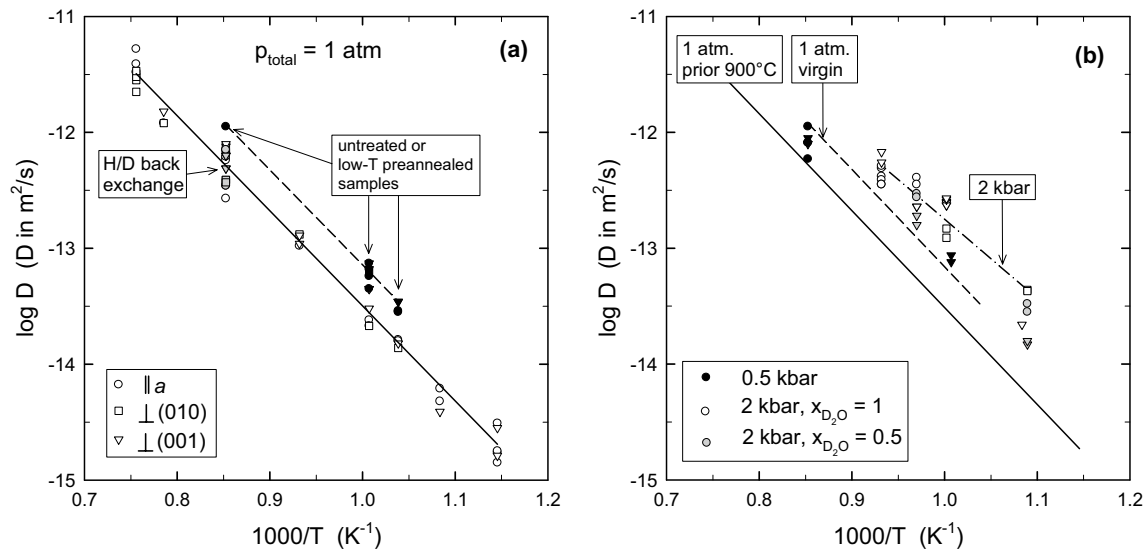


Fig. 6 **a** D/H interdiffusion in sanidine SV at 1 atm. Open symbols represent samples pre-annealed at 900 °C in air at least for 7 days. Black symbols are data for samples with no pre-treatment or pre-treatment at low temperatures. Grey symbols show the result of a H/D back-exchange experiment. Straight lines are regression for 900 °C

of 0.12 log units is close to the error of 25% (0.10 log units) estimated by error propagation considering time, temperature, variations in water content and possible slight tilting of measured profiles relative to the surface.

The untreated samples and the samples heated at low temperature form a separate trend in the Arrhenius diagram, which is parallelly shifted by +0.4 log units compared to the 900 °C pre-annealed samples, i.e. E_a values are identical at 160 kJ/mol (Table 4).

Data obtained at a water pressure of 2 kbar show a much larger scatter, but the data are still well represented by an Arrhenius relation (Fig. 6b). The larger variation in diffusion coefficients probably has experimental reasons. Embedding in powder may have not always prevent mechanical damage on the crystals during compacting. Additionally, reaction with the fluid may increase surface roughness. Often only one section could be prepared from the cuboid, and locations for profile measurement have to be carefully chosen. However, the interior of the crystals was always well preserved, i.e. no indication for alteration or melting was found by microscopy.

The activation energy for D/H interdiffusion at 2 kbar water pressure is smaller (131 kJ/mol) than at ambient pressure (Table 4). However, due to the smaller T-range and larger scatter of the data, the E_a value for 2 kbar has higher uncertainty. At 0.5 kbar only for two temperatures diffusion data were obtained. Considering the scatter of the data, this is insufficient to constrain an Arrhenius relationship.

pre-treated (solid line) and untreated or low-T pre-treated (dashed line) samples. **b** Diffusion data for 0.5 and 2 kbar. Diffusion direction is indicated by symbols (circle: parallel a; square: perpendicular (010), triangle: perpendicular (001). The dash-dotted line is a regression to the data at 2 kbar obtained with pure D₂O fluid

Effect of pressure and water fugacity

The D₂O pressure was systematically varied at a temperature of ≈ 725 °C (Fig. 7). The increase of D/H interdiffusion is particularly strong up to 2 kbar and much lower at higher pressure. A simple power law

$$\log D_{D/H} = -13.55 + 0.546 \cdot p^{0.334} \quad (6)$$

with $D_{D/H}$ in m²/s and p in kbar describes the data of D_H and D_D well ($r^2=0.83$, f.s.e. = 0.16), but other equations may also be applicable.

In the diagram, data for chemical diffusion of hydrogen derived from the $A_{OH_{total}}$ profiles are also included. The term \tilde{D}_{H_2O} is used since most likely diffusion of water molecules control the uptake and release of hydrogen as discussed below. In general, the values of \tilde{D}_{H_2O} are similar to $D_{H/D}$ for pressures up to 4 kbar (Table 3). However, below 4 kbar \tilde{D}_{H_2O} has large uncertainty due to the relatively small increase of the water content and, therefore, these data are not included in Fig. 7 and are printed in italics in Table 3. At 6 and 8 kbar, \tilde{D}_{H_2O} is systematically higher than $D_{D/H}$. As noted before, this is probably due to the loss of isotopic signature of the in-diffusing species by exchange with the stationary OH defects.

To test whether the total pressure or the fugacity of D₂O enhances the D/H exchange, two experiments were performed at 2 kbar total pressure and temperatures of 645 and

Table 4 Arrhenius parameters for D/H interdiffusion in alkali feldspars (D in m^2/s)

Feldspar	p (bar)	T range (K)	n	$\log D_0$	E_a (kJ/mol)	r^2	f.s.e	Comment
Sanidine SV	1	600–1050	42	-5.16 ± 0.14	160 ± 2.8	0.987	0.12	Pre-annealed at 900 °C
Sanidine SV	1	690–900	12	-4.79 ± 0.42	160 ± 7.9	0.976	0.07	Virgin or low-T pre-annealed
Sanidine SV	2000	645–800	23	-5.92 ± 0.60	131 ± 11.7	0.855	0.15	$p_{\text{D}_2\text{O}} = p_{\text{total}}$
Adularia A1	1	800–1050	6	-5.05 ± 0.75	162 ± 16.8	0.939	0.11	Pre-annealed at 900 °C

f.s.e. fit standard error; n number of diffusion data

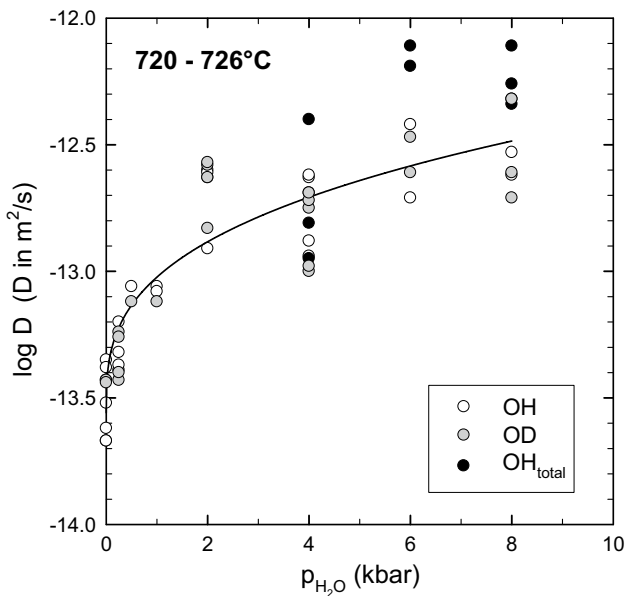


Fig. 7 Variation of diffusion coefficients of hydrogen species in sanidine SV with pressure at 720–725 °C. The trendline was obtained by fitting the data for OH and OD with a power law. See text for details

758 °C. In each experiment two capsules were used under identical p - T conditions. In one capsule the fluid phase consists of pure D_2O , in the other one a 1:1 mixture of D_2O and CO_2 was used. CO_2 was generated during heating by thermal decomposition of AgC_2O_4 . In both runs the D/H exchange was slower for the capsules containing the fluid mixture (Fig. 6b; Table 3) indicating that the fluid fugacity and not the pressure cause the increase in diffusivity. Consequently, it is inferred that the concentration of mobile hydrogen defects is increased within the crystals at elevated water fugacity.

Combined effects of pressure and temperature on D/H interdiffusion in sanidine

An attempt was made to describe the whole D/H interdiffusion data set for the sanidine SV (except for the untreated and low-T annealed samples) by a single equation combining the Arrhenius equation with a power law approach for the

dependence on D_2O pressure. For the two experiments with D_2O - CO_2 mixtures the activity of D_2O was estimated using the equation of state for pure CO_2 and H_2O (assumed to be identical to D_2O) of Pitzer and Sterner (1994) and modelling the mixing behavior according to Aranovich and Newton (1999). Calculated D_2O activities are 0.60 for run SV-E27 at 645 °C and 0.59 for run SV-E24 at 758 °C. The D_2O pressure was then calculated as the product of D_2O activity and total pressure.

Using the set of 121 data of D_H and D_D at temperatures of 600–1050 °C and pressures from 1 atm to 8 kbar, the D/H interdiffusion coefficient ($D_{D/H}$, in m^2/s) is given as follows:

$$\log D_{D/H} = -5.445 - \frac{8082.1}{T} + 0.535 \cdot p_{\text{H}_2\text{O}}^{0.3192}, \quad (7)$$

where T is the temperature in K and $p_{\text{H}_2\text{O}}$ is the water pressure in kbar. Here it is assumed that hydrogen isotopy does not affect $D_{D/H}$, i.e., $p_{\text{H}_2\text{O}}$ and $p_{\text{D}_2\text{O}}$ are equivalent. Equation (7) reproduces the experimental data with a standard error of estimate of 0.15. As shown in Fig. 8, both the 1 atm data and the high-pressure data are well reproduced by this relationship.

Equation (7) can be used to estimate the water pressure which had exerted on the natural sanidines during the last stage of their genesis. Using the diffusivity data of the virgin and low-T pre-annealed samples, re-arrangement of Eq. (7) yields a water pressure of (0.37 ± 0.13) kbar based on 17 diffusion coefficients at 3 temperatures. However, this is not more than a rough estimate, due to the large scatter of the diffusivities.

Transferability of the results to other alkali feldspars

The experiment at 800 °C, 1 atm with sanidine S2 pre-annealed for 26 d in air at 900 °C is consistent with the data of the sanidine SV (Fig. 9b). The measured D_H of $9.1 \times 10^{-14} \text{m}^2/\text{s}$ differs only by 0.09 log units from the Arrhenius line for pre-annealed SV at 1 atm. This gives confidence that the data for SV are representative for Eifel sanidines.

More interesting are the tests with the adularia A1, which shows different IR spectroscopic features than the Eifel sanidines (Behrens 2021). The shape and the

pleochroism of the OH absorption bands resembles that observed for various igneous feldspars containing *type IIa* OH defects only (Johnson and Rossman 2003, 2004). No significant change in the IR spectra was observed after heating the adularia A1 for 624 h at 900 °C in air or for 282 h at 1000 °C in steam ($p_{\text{H}_2\text{O}} = 1$ bar). This observation strongly contrasts to the Kristallina adularia studied by

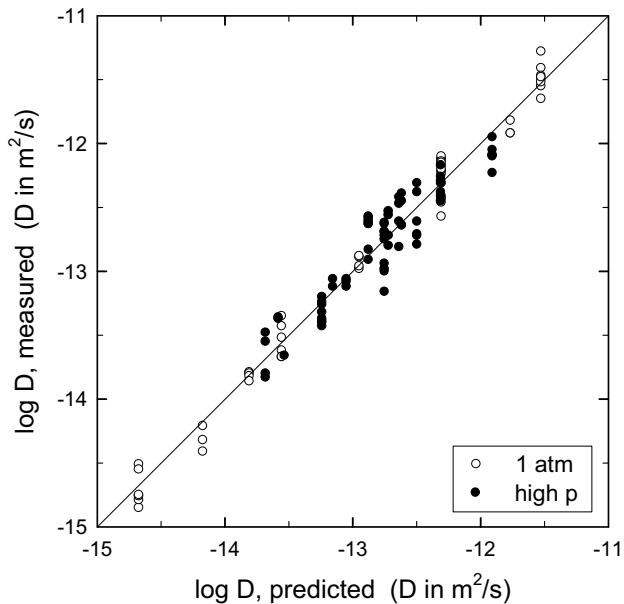


Fig. 8 Comparison of measured D/H interdiffusion coefficients with values predicted by p–T modeling using Eq. (7)

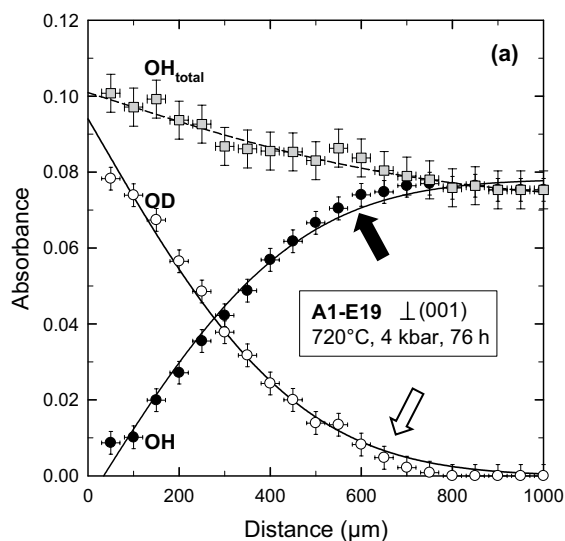


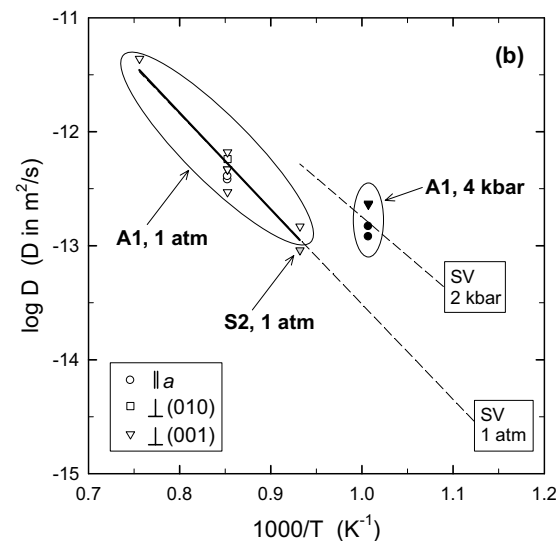
Fig. 9 Diffusion data for adularia A1 and a second Eifel sanidine S2 in comparison to the sanidine SV. **a** Profiles in A1 after an experiment at 4 kbar together with the sanidine SV shown in Fig. 5b. Note deviations of A_{OH} and A_{OD} data from the fit curve (solid lines) at greater depths (marked by arrows), which are attributed to the uptake

Kronenberg et al. (1996) for which water loss was already noticed after heating to 500 °C.

The D/H interdiffusion data for the adularia A1 at ambient pressure are in excellent agreement with the sanidine (Fig. 9b). An isotropic diffusion behavior could also be demonstrated for the adularia by an experiment with a cuboid at 900 °C (run A1-G1, Table 2). The Arrhenius relationship for the adularia (Table 4) is practically indistinguishable from that of the sanidine. Thus, an activation energy of 160 kJ/mol appears to be representative for D/H interdiffusion in alkali feldspars.

One experiment was performed with the adularia at $p_{\text{D}_2\text{O}} = 4$ kbar, simultaneously with the sanidine SV (runs A1-E19, SV-E19). The profiles are very similar in both feldspars (Fig. 4b and 9a). In both cases a systematic deviation between data and fit occurs in the crystal interior. Using the $\epsilon_{\text{OD}}/\epsilon_{\text{OH}}$ ratio of 0.85 determined for the sanidine, the total water profile was estimated for the adularia. An uptake of H_2O component is evident, but it appears to be less pronounced than for the sanidine under the same conditions (A1-E19: 31–34% increase of A_{OHtotal} ; SV-E19: 44–62% increase of A_{OHtotal}). Nevertheless, the D/H interdiffusion coefficients are very similar (Table 3). This gives confidence that Eq. (7) can be used also for other alkali feldspars with stable OH defects to estimate $D_{\text{D/H}}$ in function of T and p .

However, it should be emphasized that the direct application of the results of the present study to other potassium-rich alkali feldspars is limited to those feldspars having similar types and concentrations of water related defects. Thus, it



of water by the samples. **b** Comparison of D/H interdiffusion coefficients for the adularia A1 and a second sanidine S2 with the Arrhenius relationships derived for the sanidine SV. The bold solid line is a regression to the 1 atm data for A1

is expected that the D/H interdiffusion coefficients are higher for feldspars having a high concentration of weakly-bonded H₂O molecules (such as the Kristallina adularia studied by Kronenberg et al. 1996).

Discussion

Diffusion of hydrogen and oxygen species in feldspars

In Fig. 10 the new data for diffusion of hydrogen species in alkali feldspars are compared to literature data for hydrogen and oxygen species in feldspars. In all cases, diffusion is very strongly promoted by high water pressures. This suggests that migration of oxygen and hydrogen is correlated, at least under hydrothermal conditions.

O diffusion

A large number of data for oxygen diffusion in feldspars have been determined by isotope exchange experiments under hydrothermal and dry conditions applying different experimental and analytical techniques, see the review of Farver (2010). Only the results of Freer et al. (1997) and Derdau et al. (1998) are plotted in Fig. 10 since the authors have also studied Eifel sanidines and, hence, the data can be directly compared to those of the present study.

Under hydrothermal conditions, the O-diffusion data cover a narrow range in the log *D* vs. 1/*T* space, i.e. vary at given temperature by less than two orders of magnitude despite of different composition and genesis of feldspars (Fig. 3 in Farver 2010). Under dry conditions, the O-diffusivities are much smaller and vary considerably more. This strongly indicates different mechanisms for oxygen isotope exchange in presence and absence of water. Farver and Yund (1990) proposed that, consistent with size and charge of possible species, the dependence of oxygen diffusion on water fugacity indicates that the dominant oxygen-bearing transport species in “wet” experiments is molecular H₂O. Using computer simulation techniques, Wright et al. (1996) found that water can be accommodated in the structure of albite feldspars as both OH groups and as H₂O molecules. According to their calculations, H₂O molecules on interstitial site are the lowest energy water defects in pure albite with a solution energy of 87 kJ/mol. In the paper of Wright et al. (1996) extrinsic defects in the feldspar structure were not considered, and defect associates of H₂O molecules with vacancies may have an even lower solution energy. Wright et al. (1996) suggested that under hydrothermal conditions oxygen is transported via OH diffusion by an interstitial mechanism. But they have not made any calculations on the

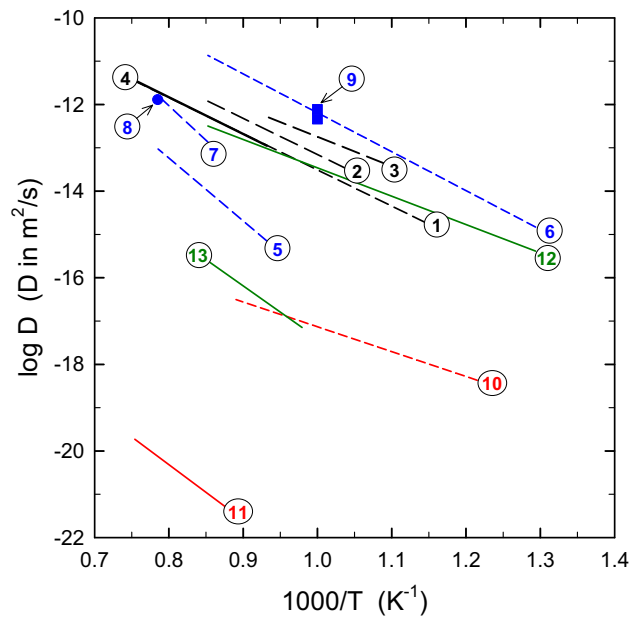


Fig. 10 Comparison of diffusion of hydrogen and oxygen species in feldspars. D/H interdiffusion is marked in black, H₂O diffusion in blue and oxygen diffusion in red. Note that only oxygen diffusion data for Eifel sanidine are considered here. For additional oxygen diffusion data and a detailed discussion see the review of Farver (2010). Tracer diffusion data for Na and K in sanidine (in green) are shown with respect to H/alkali interdiffusion processes. Data sources: [1] D-H interdiffusion, sanidine SV, pre-annealed, 1 atm, this study. [2] D-H interdiffusion, sanidine SV, virgin, 1 atm, this study. [3] D-H interdiffusion, sanidine SV, p_{H2O}=2 kbar, this study. [4] D-H, adularia A1, pre-annealed, 1 atm, this study. [5] H₂O desorption, plag An31, 1 atm, Johnson and Rossman (2013). [6] H₂O desorption, adularia, 1 atm, Kronenberg et al. (1996). [7] H₂O desorption, sanidine SV, virgin, 1 atm, Behrens (2021). [8] H₂O desorption, plag An66, 1 atm, Behrens (2021). [9] H₂O sorption, sanidine SV, p_{H2O}=6–8 kbar, this study. [10] ¹⁷O, ¹⁸O diffusion, sanidine, p_{H2O}=1 kbar, Freer et al. (1997). [11] ¹⁸O diffusion, sanidine, 1 atm, dry, Derdau et al. (1998). [12] ²²Na tracer diffusion, sanidine, 1 atm, dry, Wilangowski et al. (2015). [13] ⁴³K tracer diffusion, sanidine, 1 atm, dry, Hergemöller et al. (2017)

migration of water molecules through the feldspar structure and explicitly do not preclude such a mechanism.

According to the results of Derdau et al. (1998) oxygen diffusion in sanidine under dry conditions at 850 °C is 5 orders of magnitude slower than under hydrothermal conditions. In their experiments natural Eifel sanidine was heated in oxygen atmosphere at ambient pressure. Based on the annealing experiments of Behrens (2021), it can be expected that the mobile *type IIa* OH defects in the diffusion zone are largely eliminated, but the *type IIb* OH defects are still present. These remaining hydrogen defects appear to have no accelerating effects on O diffusion in sanidine, although the H/alkali exchange experiments of Behrens (2021) have demonstrated that hydrogen species bound in these defects are quite mobile. Most likely, the hydrogen at these conditions

moves as protons via interstitial sites with only weak interaction to network oxygen, i.e. without promoting the breaking of oxygen bridges.

Hydrogen uptake and release from feldspars.

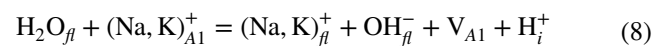
IR spectroscopy gives evidence that hydrogen is bonded to oxygen in feldspars and thus has the formal oxidation state +1. Removal or uptake of hydrogen requires charge neutrality in the feldspar interior. This can be achieved by (i) coupling to the redox state of heterovalent elements, (ii) interdiffusion of H^+ and alkali cations, and (iii) migration of neutral species, i.e. H_2O .

Interdiffusion of hydronium ions, H_3O^+ , and K^+ has been discussed also as a mechanism for hydrogen transport because of the similar size of both ions (Kronenberg et al. 1996, 1998; Doremus 1998). However, there is no spectroscopic evidence for H_3O^+ in feldspars (Johnson and Rossman 2003). Furthermore, H_3O^+ is not a rigid unit but an associate of a proton and an H_2O molecule. In feldspar, numerous other oxygen species are present to which the proton can be bound, and the proton can move independently of the water molecule.

- (i) Coupling of hydrogen to the redox state of iron is a prominent mechanism for hydrogen diffusion in olivine (Farver 2010). Rapid motion of hydrogen is possible by interdiffusion of polarons and protons, according to a reaction $Fe^{2+} + H^+ = Fe^{3+} + \frac{1}{2} H_2$. Such a mechanism is very unlikely for feldspars for two reasons: First, iron is only a trace element in feldspar ($\ll 1$ wt% Fe, Hofmeister and Rossman 1984) and, hence, the distance between Fe atoms in the feldspar structure is very high so that polaron jumps between adjacent Fe atoms are very improbable. Second, potassium-rich alkali feldspars almost exclusively contain trivalent iron (Hofmeister and Rossman 1984), and a release of hydrogen with simultaneous oxidation of divalent iron is thus not possible. Ca-rich plagioclase contain ferrous iron, but as shown by Behrens et al. (1990) oxidation of Fe^{2+} is correlated to diffusion of Na^+ and not to hydrogen species.
- (ii) Kronenberg et al. (1996) and Johnson and Rossman (2013) suggested that diffusion of H^+ via interstitial sites controlled the rate of hydrogen release from adularia and andesine in their experiments. For charge neutrality the flux of protons is compensated by a counterflux of alkali cations, i.e. Na^+ . This idea is based primarily on analogous processes in quartz that have been studied by Kats (1962). Another argument has been the similarity of the diffusivities of Na^+ and hydrogen in feldspars. The experimental

data of Johnson and Rossman (2013) were reproduced by Zhang et al. (2016) through a thermodynamic model that interconnects point defect parameters with bulk properties. Details about the nature of the point defects were not reported by Zhang et al. (2016).

As discussed below, interdiffusion of protons and alkali is certainly an important mechanism for diffusion of hydrogen species inside alkali-rich feldspars. However, such mechanism does not explain how hydrogen can be released to the atmosphere as a neutral species. To ensure charge balance, there must be available external sources and sinks for protons and alkalis. In geological settings, brine can be a source for alkali and a sink for protons. Aqueous fluids can serve as sink for alkali and source for protons. Hydrogen uptake from a fluid could occur via the following reaction:



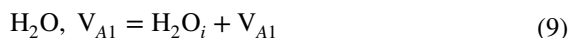
if the fluid is initially alkali-undersaturated. Here subscripts *fl*, *A1* and *i* signify the fluid phase, alkali sites and interstitial sites, respectively, and *V* indicates a vacancy.

Such a process could have occurred in the D/H exchange experiments, if the fluid has not been pre-saturated fast enough by the powder with feldspar components. However, H_2O solubility experiments of Behrens (2021), in which one molar alkali chloride solutions were used, argue against a dominant influence of reaction (8) on the H-uptake of feldspars. The water contents of samples after 24 h and 96 h at 800 °C, 2 kbar are consistent with the H_2O solubilities estimated from the diffusion runs (Fig. 11b), despite of large difference in initial alkali content of the fluids.

The IR spectra recorded after the 6 kbar and 8 kbar experiments do not give a clear indication for the formation of new types of hydrogen species. The OD band is at same position (2520 cm^{-1} , measured on (010) and (001) sections with $E_{\text{dom}} \parallel a$) than after D/H exchange at ambient pressure, and in the water-enriched region of the crystal the OH vibrations bands are too weak for detailed analyses. Detecting changes in IR spectra is also complicated by the fact that the increase in water content is relatively small. Compared to the natural sanidine with $129 \pm 10 \text{ } \mu\text{g/g } H_2O$, the water content is only 26% higher in the 8-kbar experiment.

- (iii) Diffusion of H_2O molecules is nowadays a widely accepted mechanism for the transport of hydrogen species in silicate and aluminosilicate glasses and melts (Behrens et al. 2007; Zhang and Ni 2010). Jumps of H_2O molecules between interstitial sites as a possible mechanism for diffusion of hydrogen and

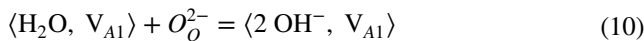
oxygen species has been discussed also for feldspars (e.g. Farver and Yund 1990; Kronenberg et al. 1996, 1998; Wright et al. 1996; Doremus 1998; Behrens 2021). The open structure of the aluminosilicate network in feldspars offers numerous interstitial sites which potentially can host H₂O molecules (Wright et al. 1996). Furthermore, vacancies on alkali sites can be occupied by water molecules (Beran 1986; Kronenberg et al. 1996; Behrens 2021). Interstitial water, H₂O_i, is very mobile while H₂O molecules located on V_{Al} sites, H₂O, V_{Al}, are stationary defects. The conversion of these defects can be described by the reaction



Structural H₂O has been found in feldspars such as microcline and some adularia that were formed or transformed at relatively low temperatures (Johnson and Rossman 2004). Upon heating, these defects were irreversibly destroyed in studies of Aines and Rossman (1985) and Kronenberg et al. (1996), demonstrating that these defects are thermodynamically instable under magmatic conditions.

In volcanic feldspars, OH groups are the predominant hydrous species (Johnson and Rossman 2003, 2004; Behrens 2021). In the context of the defect model proposed here, this can be explained by a reaction of the water molecule

with neighboring oxygen, O_O²⁻, and the formation of a pair of OH groups



As long as the OH groups do not diffuse apart, a mobile H₂O molecule can be formed again very easily by back reaction. Hence, the combined reactions (9) and (10) determine the concentration of H₂O_i in the interior of feldspar and, thus, have major impact on hydration and dehydration kinetics.

The term V_{Al} implies that a single type of cation vacancy is involved in the H₂O-hosting defect. However, different types of vacancies can be present in a complex mineral such as feldspar. The effective charge of the vacancy can be very variable and is determined by the Al/Si ratio on the surrounding tetrahedral sites as well as the charges of the neighboring cations. Assuming a perfect network structure, Kronenberg et al. (1996) suggested that in Kristallina adularia a negatively charged vacancy on an alkali site is compensated by a divalent cation such as Ba²⁺ or Ca²⁺ in the immediate vicinity. On the other hand, neutral vacancies can result from incorporation of an excess of SiO₂ compared to the ideal feldspar composition (Behrens et al. 1990; Behrens 2021). Formally, this corresponds to mixing with a feldspar analog component V_{Al}Si₄O₈.

The formation of mobile H₂O is more difficult if the hydrogen defects consist of isolated OH groups. This is

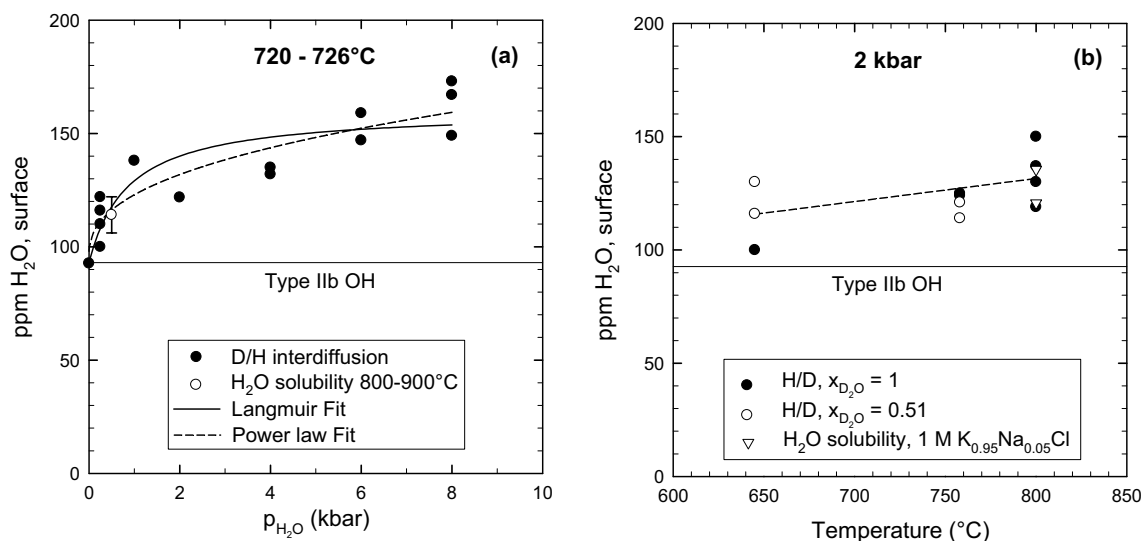


Fig. 11 a, b Total water content at the sample surface of sanidine SV after high pressure diffusion experiments. The thin solid line represents water incorporated as *type IIb OH* defects (Behrens 2021). **a** At constant temperature close to 725 °C. The data at 2 kbar is based on the regression in (a). The average of 6 H₂O solubility experiments at 800–900 °C, 0.5 kbar (Behrens 2021) is shown for comparison. Both, fittings by a Langmuir equation and a power law are illustrated. **b** At

constant total pressure of 2 kbar. Data with lower x_{D2O} in the fluid show no systematic deviation from data with pure D₂O fluid and, thus, a single regression is used to describe the T dependence. Results of H₂O solubility experiments with 1 molar alkali chloride solutions from Behrens (2021) are included for comparison. Estimated error of data from diffusion experiments is ≈ 20 ppm. See text for discussion

probably the case with *type IIb OH* defects in sanidine. Analogous to quartz, a substitution of Si^{4+} by Al^{3+} and H^+ has been proposed as the incorporation mechanism for these defects (Behrens 2021). From alkali/H exchange and back exchange experiments, it was concluded that the protons are located on interstitial sites (H_i^+). Two such defects must come together by diffusion for the formation of H_2O_i



This reaction creates energetically unfavorable oxygen vacancies, V_o , that act as traps for interstitial H_2O . As a consequence, the dehydration kinetics slow down with proceeding dehydration. This explains the difficulty in completely dehydrating the sanidines and the absence of profiles in partially dehydrated samples (Behrens 2021).

The adularia A1 has distinctly different IR spectra than the sanidine (Behrens 2021). Using the terminology of Johnson and Rossman (2004) the hydrogen species are typical *IIa OH* defects. Hydrogen is also very tightly bound in the adularia, and no significant H loss of the adularia was observed even after annealing mm thick plates at 900 °C in air for weeks. This suggests that isolated OH groups are the dominant hydrogen species in this mineral as well. These findings emphasize that the IR spectroscopically defined types of hydrogen species tell us little about the actual bond strengths.

The defect models can be used to explain H_2O diffusivities in feldspars plotted in Fig. 10. The higher diffusivities and lower activation energy of the adularia of Kronenberg et al. (1996) compared to the andesine of Johnson and Rossman (2013) can be attributed to the instability of the hydrogen defects in the adularia. Since the defect centers are irreversibly destroyed in the adularia, they cannot act as traps for diffusing H_2O molecules, and reaction (12) proceeds only to the right. Thus, the local concentration of H_2O_i , determined by the dissociation rate of the H_2O , V_{A1} defects as well as the mobility of H_2O_i , is high in the adularia. In the andesine, with proceeding dehydration the concentration of V_{A1} and, hence, the probability for the back-reaction increases. Therefore, the effective H_2O diffusivity is expected to decrease with degree of dehydration. Such effect may explain the deviation between measured data points and loss curve at long run duration/large hydrogen loss in the study of Johnson and Rossman (2013). The loss curve was calculated with the assumption of constant diffusivity.

Dehydration is one order of magnitude faster for a labradorite An66 and the sanidine SV compared to the andesine (Behrens 2021). In terms of the defect model, this implies that H_2O molecules are less strongly bound to V_{A1} in the labradorite and in the sanidine than in the andesine. The evolution of the water content of the labradorite with time could be well described assuming a constant diffusion coefficient

which is also consistent with weak bonding of the H_2O molecules to the vacancies.

A rapid water release was observed for the sanidine only in the initial stage of dehydration up to a water loss of approx. 25%. The removal of the residual water was extremely slow and complete dehydration of 0.7–0.9 mm thick sections was not achieved at 1000 °C even after annealing for 108 days in air dried by phosphorus pentoxide (Behrens 2021). No attempt was made to quantify the diffusion coefficients from these data. But the concentration dependence of $\tilde{D}_{\text{H}_2\text{O}}$ is in any case much more pronounced in the sanidine than in the andesine and the labradorite due to the back reaction of (11). Similar behavior can be expected for the adularia, although this has not been studied in detail.

The $\tilde{D}_{\text{H}_2\text{O}}$ values derived from uptake of water in the D/H exchange experiments with the sanidine SV at ≈ 720 °C and pressures of 4–8 kbar are three orders of magnitude higher than extrapolated values for the initial dehydration at 1 atm based on line 7 in Fig. 11. This suggests a correspondingly large increase in mobile hydrogen species, although C_w at the surface had increased by no more than 34%. That is, the relative abundance of mobile hydrogen species has been drastically increased by water uptake. The A_{OHtotal} profiles of sanidine in Fig. 4a–d and adularia in Fig. 9a are well fitted assuming a constant $\tilde{D}_{\text{H}_2\text{O}}$. But the shape of the profiles is consistent also with a weak dependence of $\tilde{D}_{\text{H}_2\text{O}}$ on C_w . It is striking that the $\tilde{D}_{\text{H}_2\text{O}}$ value of the sanidine at 720 °C, 4–8 kbar is similar to the hydrogen diffusivity in the Kristallina adularia of Kronenberg et al. (1996). This suggests that a high concentration of mobile hydrogen species can be produced by both an internal dissociation reaction and a high water fugacity.

D/H interdiffusion

The activation energy for oxygen diffusion and D/H interdiffusion in Eifel sanidine under hydrothermal conditions is very similar (109.7 ± 4 kJ/mol for oxygen diffusion at 1 kbar, 130.7 ± 11.7 kJ/mol for D/H interdiffusion at 2 kbar). This supports the hypothesis that hydrogen and oxygen isotopes are transported by the same carrier at these conditions. For these pressures, the A_{OH} and A_{OD} profiles in this study and the ^{18}O and ^{17}O profiles in Freer et al. (1997) can be well fitted by the corresponding solution of Fick's 2nd law assuming a constant diffusion coefficient. A prerequisite for this approach is that local equilibrium is established between the mobile and stationary species or, in other words, the exchange rate between mobile and stationary species is high compared to the jump frequency of the mobile species.

For these boundary conditions, the apparent diffusivities, $D_{\text{D/H}}$ and D_o are related to the diffusivity of the mobile species $D_{\text{H}_2\text{O},m}$ by the relative abundance of the species:

$$C_w \cdot D_{D/H} = C_{H_2O,m} \cdot D_{H_2O,m} \quad (12)$$

$$C_O \cdot D_O = C_{H_2O,m} \cdot D_{H_2O,m} \quad (13)$$

where C_w and C_O are the water content and the oxygen content, respectively and $C_{H_2O,m}$ is the unknown content of the mobile species H_2O_i . Combining Eqs. (12) and (13), the ratio of the diffusion coefficients should be given by the concentration ratio oxygen atoms in the feldspar and dissolved water:

$$\frac{D_{D/H}}{D_O} = \frac{c_O}{c_w} \quad (14)$$

Using Eq. (7) to calculate $D_{D/H}$, the $D_{D/H}/D_O$ ratio equals 19,900 at 800 °C, 1 kbar. The C_O/C_w ratio in the natural sanidine SV is 4012, based on the IR calibration of Johnson and Rossman (2004) and the EMPA data in Table 1. This is lower by a factor of 5 than the experimental $D_{D/H}/D_O$ ratio at 800 °C, 1 kbar. An inaccuracy of the water content cannot explain such large deviation. Application of the IR calibration of Mosenfelder et al. (2015) results in 40% lower C_w for the sanidine, while nuclear reaction analysis yielded 50% higher C_w . Thus, the most likely explanation is that not only H_2O molecules are mobile hydrogen species. Considering the alkali/H exchange experiments of Behrens (2021), migration of protons also contributes to the hydrogen isotope exchange.

At ambient pressure in pre-annealed sanidine, H_2O_i is negligible and proton migration is the determining factor for the hydrogen isotope exchange rate. Interdiffusion of protons and alkali cations is the most probable mechanism. Tracer-diffusion data of Wilangowski et al. (2015) and Hergemöller et al. (2017) show that K diffusion is too slow in the sanidine, but Na diffusion is very similar to D/H interdiffusion (Fig. 10). Activation energies for Na diffusion (125 kJ/mol) and D/H interdiffusion in pre-annealed sanidine (150 kJ/mol) are also comparable. Electrical conductivity measurements on single crystals also support that the charge transport in the sanidine is determined by the mobility of Na (El Maanaoui et al. 2016). This supports the idea that under dry conditions hydrogen transport in alkali feldspars occurs via Na/H interdiffusion.

“Water solubility” in alkali feldspars

As stated in the previous work (Behrens 2021), the water content of feldspars is not only determined by water fugacity, pressure and temperature, but is significantly influenced by pre-existing defects in the crystals. Often the defects were already incorporated into the structure during crystal

growth, but they may have been also formed later by alteration or diffusion. Hence, the term “water solubility” is not universal for feldspars, and the ability to absorb or to release water depends on the type and concentration of defects in the feldspar structure.

In the previous study, the solubility of water in volcanic feldspars was tested by annealing crystals at controlled water pressure and temperature for variable times (Behrens 2021). From the evolution of water contents with p_{H_2O} , it was concluded that two types of hydrogen defects are present in Eifel sanidines. A very stable hydrogen defect reaches its saturation already at $p_{H_2O} > 100$ mbar at 1000 °C. A possible explanation of this defect is the coupled substitution of $Al^{3+} + H^+$ for Si^{4+} , a common substitution pattern in quartz minerals (e.g., Kats 1962). Above $p_{H_2O} = 300$ mbar, the water content of Eifel sanidine strongly increases by formation of a second hydrogen-bearing defect which is less stable and, hence, strongly promoted by water pressure. To prevent melt formation, only relatively low pressures of up to 16 bar were applied in the study of Behrens (2021) on water solubility in sanidine at 1000 °C. The obtained data do not allow to constrain whether the H_2O solubility continuously increase with p_{H_2O} at high pressures or a saturation value is reached.

The D/H interdiffusion experiments revealed additional information on the pressure dependence of the solubility of H_2O in sanidine. If diffusion controls the uptake of hydrogen species from the fluid, the water content of the feldspar at contact with the fluid can be assumed to represent the equilibrium solubility of H_2O in the feldspar. Hence, the fitting parameter A_s in Eq. (2) can be used to estimate the H_2O solubility.

As shown in Fig. 11a, the increase of water solubility with p_{H_2O} is particularly pronounced between 0 and 1 kbar, and the trend flattens at higher pressure. Data from water solubility experiments at 500 bar and temperatures of 800 and 900 °C from Behrens (2021) are consistent with the diffusion-based data. The temperature dependence of water solubility is low (Fig. 11b), so that the temperature deviation between solubility and diffusion experiments is insignificant. However, it has not been clearly demonstrated that equilibrium was reached after 240–480 h in the solubility runs because no systematic time variation was performed by Behrens (2021).

A constant solubility level at p_{H_2O} is expected if a fixed number of equivalent sites is available for water molecules. This corresponds to the Langmuir model for gas adsorption on surfaces. On the other hand, a continuous increase is expected in the case of energetically different sites to host water molecules. Sites with strong bonding of the H_2O molecules are already occupied at low pressures, while those with weak bonding are only occupied at higher pressures. Such

conditions can be described, for example, with a power-law approach.

The data show a trend of a continuous increase of water solubility with pressure up to 8 kbar at 720–725 °C. However, due to the large scatter of the data, it is not possible to prove such trend unambiguously. Both, the Langmuir fit

$$C_w = 93 + 0.0778 \cdot p_{\text{H}_2\text{O}} / (1 + 0.001556 \cdot p_{\text{H}_2\text{O}}), r^2 = 0.77, \text{ f.s.e. of } 10.4 \mu\text{g/g} \quad (15)$$

and the power law fit

$$C_w = 95.32 + 1.695 \cdot p_{\text{H}_2\text{O}}^{0.404}, r^2 = 0.84, \text{ f.s.e. of } 12.0 \mu\text{g/g} \quad (16)$$

describe the trend of the data with similar precision, i.e., when considering the estimated error of the data of $\pm 20 \mu\text{g/g}$. In these equations, C_w is in $\mu\text{g/g}$ and $p_{\text{H}_2\text{O}}$ in kbar. The power law is more consistent with the discussed defect models and the diffusion data in Fig. 7 and is therefore preferred.

There appears to be a small positive effect of temperature on H_2O solubility at 2 kbar, but again the uncertainty of the data is too high to prove such trend (Fig. 10b). This becomes obvious when comparing the runs using $\text{D}_2\text{O}/\text{CO}_2$ mixtures with those using pure D_2O . A higher water content is expected for the experiments with pure D_2O fluids due to higher D_2O fugacity but the data at 645 °C show the opposite trend. Thus, the experimental data are also consistent with a T-independent H_2O solubility. Assuming a temperature-independent water solubility, we can estimate from the two fit curves that the water content of the natural sanidine of 129 $\mu\text{g/g}$ corresponds to an equilibrium water pressure of 1–2 kbar in the late stage of the sanidine before eruption.

Conclusions

The mobility of hydrogen species in feldspars is strongly related to pre-existing defects in the feldspar structure. From the D/H exchange experiments it is inferred that isolated OH groups in the sanidine and the adularia can mobilize protons via Na/H interdiffusion but H_2O is difficult to release since unfavored defects such as oxygen vacancies are formed. Comparison to oxygen diffusion data of Freer et al. (1997) implies that under hydrothermal conditions both H_2O molecules and protons contribute to the transport of hydrogen in alkali feldspars. In-diffusing H_2O is stored to large extent as an associate with pre-existing defects, probably vacancies on alkali sites. Variation of D/H interdiffusion coefficients and surface concentration of water in the crystals with pressure indicate that the defects have different bond strength for H_2O

molecules. Since the defects with strong bonding of H_2O are saturated first, the mobility of the water molecules increases with increasing water content.

For complex minerals such as feldspars an unequivocal interpretation of experimental diffusion data is often not possible, i.e., when considering the uncertainty of the data and

the variability of major and trace element composition as well as structural states (e.g. degree of Al/Si ordering). To test the proposed defect models and diffusion mechanism, additional research is required. The measured data provided in the electronic supplement may be used for a more in-depth modelling of the diffusion processes. A promising approach for further clarification is also computer simulation, which has largely improved in the last decades.

Water solubilities derived from diffusion profiles and from solubility experiments show that feldspars are difficult to use as hygrometers. The water contents of the feldspars are essentially determined by extrinsic defects, which were often already incorporated during crystallization. The nature and concentration of these defects is often poorly constrained, making direct conclusions about the water fugacity of a magma from measured water contents of feldspars nearly impossible. Extensive experimental tests and defect studies are necessary to calibrate the method for specific feldspars. This is very demanding and, in most cases, not feasible.

Supplementary Information The online version contains supplementary material available at <https://doi.org/10.1007/s00269-021-01150-w>.

Acknowledgements My special thanks go to Otto Dietrich for the excellent preparation of feldspar sections. I thank Fabian Hergemöller for stimulating thoughts on proton and alkali diffusion. Two anonymous reviewers are acknowledged for carefully reading the manuscript and given useful advices. The research was supported by researcher unit FOR2881 of the German Science foundation (DFG).

Funding Open Access funding enabled and organized by Projekt DEAL.

Open Access This article is licensed under a Creative Commons Attribution 4.0 International License, which permits use, sharing, adaptation, distribution and reproduction in any medium or format, as long as you give appropriate credit to the original author(s) and the source, provide a link to the Creative Commons licence, and indicate if changes were made. The images or other third party material in this article are included in the article's Creative Commons licence, unless indicated otherwise in a credit line to the material. If material is not included in the article's Creative Commons licence and your intended use is not permitted by statutory regulation or exceeds the permitted use, you will need to obtain permission directly from the copyright holder. To view a copy of this licence, visit <http://creativecommons.org/licenses/by/4.0/>.

References

- Aines RD, Rossman GR (1985) The high temperature behavior of trace hydrous components in silicate minerals. *Am Miner* 70:1167–1179
- Aranovich LY, Newton RC (1999) Experimental determination of CO₂-H₂O activity-composition relations at 600–1000°C and 6–14 kbar by reversed decarbonation and dehydration reactions. *Am Miner* 84:1319–1332
- Baschek G, Johannes W (1995) The estimation of NaSi-CaAl interdiffusion rates in peristerites by homogenization experiments. *Eur J Miner* 7:295–330
- Behrens H (2021) Hydrogen defects and water solubility in igneous feldspars. *Phys Chem Miner* 48:8
- Behrens H, Johannes W, Schmalzried H (1990) On the mechanisms of cation diffusion processes in ternary feldspars. *Phys Chem Miner* 17:62–78
- Behrens H, Zhang Y, Leschik M, Wiedenbeck M, Heide G, Frischat GH (2007) Molecular H₂O as carrier for oxygen diffusion in hydrous silicate melts. *Earth Planet Sci Lett* 254:69–76
- Beran A (1986) A model of water allocation in alkali feldspar, derived from infrared-spectroscopic investigations. *Phys Chem Miner* 13:306–310
- Crank J (1975) *The mathematics of diffusion*, 2nd edn. Clarendon Press, Oxford, p 414
- Derdau D, Freer R, Wright K (1998) Oxygen diffusion in anhydrous sanidine feldspar. *Contrib Miner Pet* 133:199–204
- Doremus RH (1998) Comment on “Stationary and mobile hydrogen defects in potassium feldspar.” *Geochim Cosmochim Acta* 62:377–378
- El Maanaoui H, Wilangowski F, Maheshwari A, Wiemhöfer HD, Abart R, Stolwijk NA (2016) Ionic conductivity in gem quality single-crystal alkali feldspar from the Eifel: temperature-, orientation-, and composition dependence. *Phys Chem Miner* 43:327–340
- Elphick SC, Graham CM, Dennis PF (1988) An ion microprobe study of anhydrous oxygen diffusion in anorthite: a comparison with hydrothermal data and some geological implications. *Contrib Mineral Pet* 100:490–495
- Farver JR (2010) Oxygen and hydrogen diffusion in minerals. *Rev Miner Geochem* 72:447–507
- Farver JR, Yund RA (1990) The effect of hydrogen, oxygen and water fugacity on oxygen diffusion in alkali feldspar. *Geochim Cosmochim Acta* 54:2953–2964
- Freer R, Wright K, Kroll H, Göttlicher J (1997) Oxygen diffusion in sanidine feldspar and a critical appraisal of oxygen isotope-mass-effect measurements in non-cubic materials. *Phil Mag* A75:485–503
- Giletti BJ, Semet MP, Yund RA (1978) Studies in diffusion-III. oxygen in feldspars: an ion microprobe determination. *Geochim Cosmochim Acta* 42:45–57
- Goldsmith JR (1991) Pressure-enhanced Al/Si diffusion and oxygen isotope exchange. In “Diffusion, atomic ordering and mass transport” ed. Ganguly J *Adv Phys Geochem* 8:221–247
- Hergemöller F, Wegner M, Deicher M, Wolf H, Brenner F, Hutter H, Abart R, Stolwijk NA (2017) Potassium self-diffusion in a K-rich single-crystal alkali feldspar. *Phys Chem Miner* 44:345–351
- Hofmeister AM, Rossman GR (1984) Determination of Fe³⁺ and Fe²⁺ concentrations in feldspar by optical absorption and EPR spectroscopy. *Phys Chem Minerals* 11:213–224
- Johnson EA (2006) Water in nominally anhydrous crustal minerals: Speciation, concentration, and geologic significance. *Rev Mineral Geochem* 62:117–154
- Johnson EA, Rossman GR (2003) The concentration and speciation of hydrogen in feldspars using FTIR and 1H MAS NMR spectroscopy. *Am Miner* 88:901–911
- Johnson EA, Rossman GR (2004) A survey of hydrous species and concentrations in igneous feldspars. *Am Miner* 89:586–600
- Johnson EA, Rossman GR (2013) The diffusion behavior of hydrogen in plagioclase feldspar at 800–1000 °C: implications for reequilibration of hydroxyl in volcanic phenocrysts. *Am Miner* 98:1779–1787
- Kats A (1962) Hydrogen in alpha quartz. *Phillips Res Repts* 17:201–279
- Kronenberg AK, Yund RA, Rossman GR (1996) Stationary and mobile hydrogen defects in potassium feldspar. *Geochim Cosmochim Acta* 60:4075–4094
- Kronenberg AK, Yund RA, Rossman GR (1998) Reply to the comment by Robert H. Doremus on “stationary and mobile hydrogen defects in potassium feldspar.” *Geochim Cosmochim Acta* 62:379–382
- Matsuda K (2020) Frictional properties of anorthite (feldspar): implication for the lower boundary of the seismogenic zone. *Earth Planet Space* 72:135
- Matsuda K, Arai T, Takahashi M (2019) Effects of frictional properties of quartz and feldspar in the crust on the depth extent of the seismogenic zone. *Progr Earth Planet Sci* 6:50
- Mosenfelder JL, Rossman GR, Johnson EA (2015) Hydrous species in feldspars: a reassessment based on FTIR and SIMS. *Am Miner* 100:1209–1221
- Pitzer KS, Sterner SM (1994) Equation of state valid continuously from zero to extreme pressures for H₂O and CO₂. *J Chem Phys* 102:3111–3116
- Rybacki E, Gottschalk M, Wirth R, Dresen G (2006) Influence of water fugacity and activation volume on the flow properties of fine-grained anorthite aggregates. *J Geophys Res* 111:B03203
- Smith JV (1974) *Feldspar minerals. I. Crystal structure and physical properties*. Springer-Verlag, New York, p 1627
- Wilangowski F, Abart R, Divinski SV, Stolwijk NA (2015) Radiotracer experiments and monte carlo simulations of sodium diffusion in alkali feldspar: evidence against the vacancy mechanism. *Defect Diffus Forum* 363:79–84
- Wright K, Freer R, Catlow CRA (1996) Water-related defects and oxygen diffusion in albite: a computer simulation study. *Contrib Miner Pet* 125:161–166
- Yang X, Keppler H, McCammon C, Ni H (2012) Electrical conductivity of orthopyroxene and plagioclase in the lower crust. *Contrib Miner Pet* 163:33–48
- Yund RA (1986) Interdiffusion of NaSi-CaAl in peristerite. *Phys Chem Miner* 13:11–16
- Yund RA, Anderson TF (1974) The effect of fluid pressure on oxygen isotope exchange between feldspar and water. *Geochim Cosmochim Acta* 42:235–239
- Yund RA, Tullis J (1980) The effect of water, pressure and strain on Al/Si order-disorder kinetics in feldspar. *Contrib Miner Pet* 72:297–302
- Zhang Y, Ni H (2010) Diffusion of H, C and O components in silicate melts. *Rev Mineral Geochem* 72:171–225
- Zhang B, Shan S, Wu X (2016) H, Na, and K diffusion in plagioclase feldspar by relating point defect parameters to bulk properties. *Phys Chem Miner* 43:151–159